iScience

CellPress
OPEN ACCESS

Article

Vascular smooth muscle cell dysfunction contribute to neuroinflammation and Tau hyperphosphorylation in Alzheimer disease

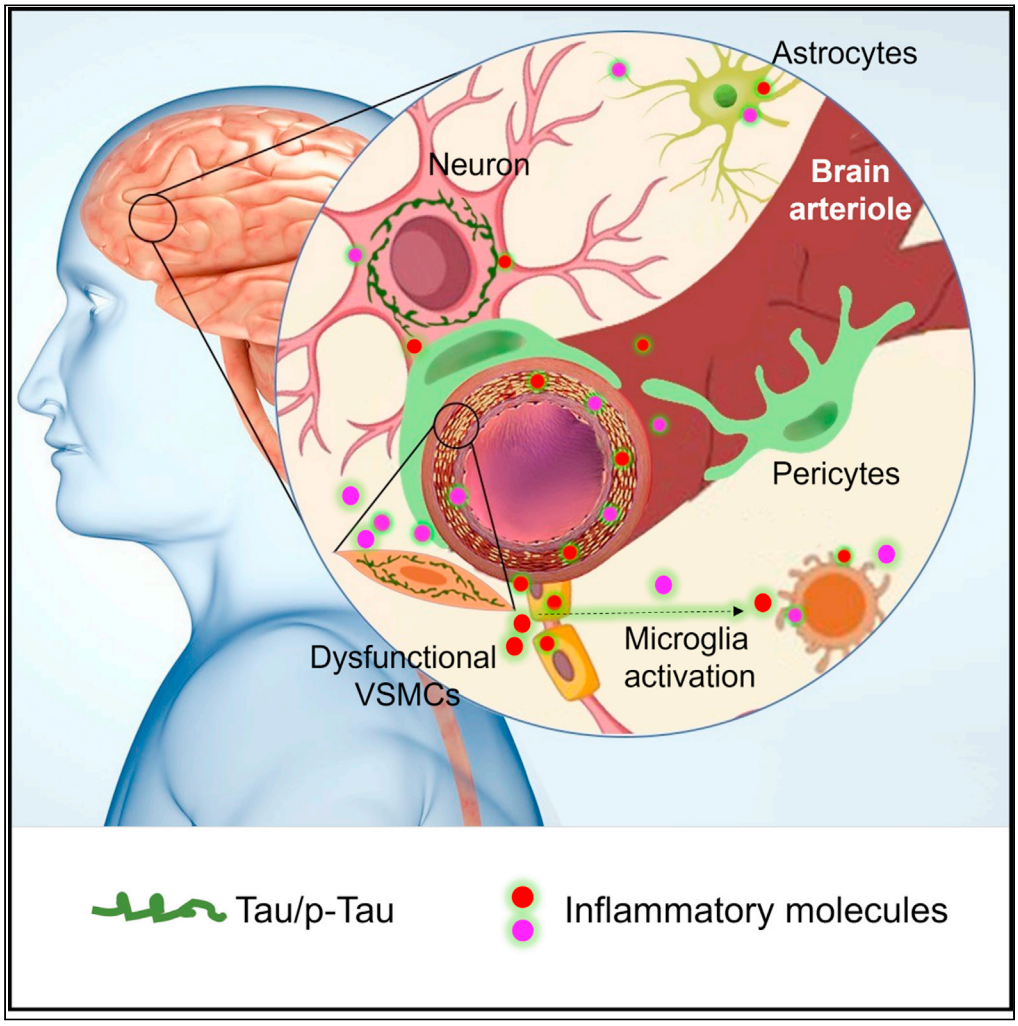

Jorge A. Aguilar-Pineda, Karin J. Vera-Lopez, Pallavi Shrivastava, ..., Rajeev Malhotra, Mark E. Lindsay, Christian L. Lino Cardenas

clinocardenas@mgh.harvard.edu

Highlights

Loss of VSMC contractile phenotypes correlates with Tau accumulation in brain arterioles

VSMC dysfunction promotes the hyperphosphorylation of Tau protein at multiple residues

VSMC dysfunction occurs in an age-dependent manner in brain arterioles of patients with AD

Vascular smooth muscle cell is a promising therapeutic target in AD

Aguilar-Pineda et al., iScience *24*, 102993
September 24, 2021
https://doi.org/10.1016/j.isci.2021.102993

iScience

CellPress
OPEN ACCESS

Article

Vascular smooth muscle cell dysfunction contribute to neuroinflammation and Tau hyperphosphorylation in Alzheimer disease

Jorge A. Aguilar-Pineda,[2] Karin J. Vera-Lopez,[2] Pallavi Shrivastava,[2] Miguel A. Chávez-Fumagalli,[2] Rita Nieto-Montesinos,[2] Karla L. Alvarez-Fernandez,[2] Luis D. Goyzueta Mamani,[2] Gonzalo Davila Del-Carpio,[2] Badhin Gomez-Valdez,[2] Clint L. Miller,[3] Rajeev Malhotra,[1] Mark E. Lindsay,[1] and Christian L. Lino Cardenas[1,2,4,*]

SUMMARY

Despite the emerging evidence implying early vascular contributions to neurodegenerative syndromes, the role of vascular smooth muscle cells (VSMCs) in the pathogenesis of Alzheimer disease (AD) is still not well understood. Herein, we show that VSMCs in brains of patients with AD and animal models of the disease are deficient in multiple VSMC contractile markers which correlated with Tau accumulation in brain arterioles. *Ex vivo* and *in vitro* experiments demonstrated that VSMCs undergo dramatic phenotypic transitions under AD-like conditions, adopting pro-inflammatory phenotypes. Notably, these changes coincided with Tau hyperphosphorylation at residues Y18, T205, and S262. We also observed that VSMC dysfunction occurred in an age-dependent manner and that expression of Sm22α protein was inversely correlated with CD68 and Tau expression in brain arterioles of the 3xTg-AD and 5xFAD mice. Together, these findings further support the contribution of dysfunctional VSMCs in AD pathogenesis and nominate VSMCs as a potential therapeutic target in AD.

INTRODUCTION

Alzheimer disease (AD) is a debilitating neurological disorder that leads to cognitive decline and dementia. The prevalence of patients with AD is predicted to surge more than 150% in the next decade, in line with the increased aging in US population (>65 years old) (Agarwal et al., 2020; Alzheimer's Association, 2018). Tau neurofibrillary tangle (NFT) deposits are characteristic hallmarks of AD and correlate closely with cognitive decline which begins to develop around two decades before clinical manifestations (Nirzhor et al., 2018; Leszek et al., 2003; Barthélemy et al., 2020). The microtubule-associated Tau protein plays a key role in morphogenesis and homeostasis of mature neurons. Also, multiple residues in the Tau protein (~80 aa) undergo posttranslational modifications (PTMs), which are critical for proper assembly and stability of the microtubule cytoskeleton, transport of nutrients, protein synthesis, neuroprotection, and apoptosis (Wesseling et al., 2020). However, aberrantly increased levels of soluble Tau protein often leads to intracellular toxicity. Likewise, excessive phosphorylation results in the self-assembly of tangles and straight filaments, which are involved in the physio-pathogenesis of AD-related neurodegenerative tauopathies, such as frontotemporal dementia, progressive supranuclear palsy (PSP), and corticobasal degeneration (Lathuilière et al., 2017).

Recent proteomics studies have identified over 50 candidate Tau phosphorylation sites during Tau aggregation into neurofibrillary tangles, supporting a critical role of Tau PTMs in AD progression (Barthélemy et al., 2019; Wesseling et al., 2020). The recent discoveries of Tau hyperphosphorylation sites have led to the development of biomarkers for the diagnosis of Tau-associated diseases. Indeed, Tau hyperphosphorylation at residues T153, T205, S208, and T217 was exclusively found in the CSF of patients with AD (Barthélemy et al., 2019). Also, increased plasma levels of p-Tau (T181) were used to stratify patients with AD dementia from non-AD neurodegenerative diseases (Janelidze et al., 2021). The hyperphosphorylation of residues T181 and T217 was shown to occur decades before the formation of neurofibrillary tangles (NFT) and onset of clinical symptoms (Barthélemy et al., 2020). And t-Tau and p-Tau (T205) were associated with brain atrophy, cognitive decline, and late onset of symptoms. In addition,

[1]Cardiovascular Research Center, Cardiology Division, Massachusetts General Hospital, Boston, MA 02114, USA

[2]Laboratory of Genomics and Neurovascular Diseases, Vicerrectorado de investigacion, Universidad Catolica de Santa Maria, Arequipa, Peru

[3]Center for Public Health Genomics, Department of Public Health Sciences, University of Virginia, Charlottesville, VA 22908, USA

[4]Lead contact

*Correspondence: clinocardenas@mgh.harvard.edu

https://doi.org/10.1016/j.isci.2021.102993

hyperphosphorylation at Y18 residue is increased in the cortex at Braak stage V/VI in patients with AD (Neddens et al., 2018). Those clinical observations indicate that phosphorylation alterations in the Tau protein follow a strict curve over the course of AD progression (Barthélemy et al., 2020). Genetically, several mutations in the Tau gene have been shown to cause neurodegenerative disorders including familial frontotemporal dementia and PSP and parkinsonism linked to chromosome 17 (FTDP-17) (López-González et al., 2016; Morishima-Kawashima, 2001). The well-studied mutated Tau^{P301L} was first diagnosed in six French families with frontotemporal dementia and parkinsonism (Dumanchin et al., 1998) and has since been found in approximately 32 families around the world (Tsuboi, 2004; Kowalska, 2009). This proline-to-leucine substitution causes Tau aggregation and develops numerous intracytoplasmic tau deposits in multiple brain regions, including the hippocampus, neocortex, and substantia nigra (Giménez-Llort et al., 2008).

Vascular dementia (VD) is the second most common subtype of dementia after AD, accounting for 15–30% of dementia cases globally (Lobo et al., 2000; Rizzi et al., 2014; Jhoo et al., 2008; Chan et al., 2013; Kalaria et al., 2008). Recent epidemiological studies have established a link between AD and cardiovascular disease (CVD) risk factors (Lamar et al., 2020) (e.g., hypertension, atherosclerosis, obesity, type 2 diabetes, etc.), suggesting that the neurovascular units (NVUs) may contribute to the initiation and progression of AD (Zlokovic, 2011; Kim et al., 2020). These emerging data suggest that AD is a multifactorial, multi-organ disease with triggers beyond the CNS unit including vascular dysfunction and inflammation, which may precede neuropathological changes (De la Torre et al., 2018). In this context, vascular smooth muscle cells (VSMCs) may play fundamental roles in regulating disease processes underlying both CVDs and AD (Frismantiene et al., 2018; Mok et al., 2006).

VSMCs are highly plastic cells in the vessel wall (Castro et al., 2018; Rong et al., 2003) and readily transition from a contractile state to a synthetic or transdifferentiated entity in response to a wide range of pathogenic stimulus (Wang et al., 2015; Owens, 1995; Kalaria, 2003; Erkinjuntti et al., 2004). Transdifferentiated VSMCs are often characterized by loss of expression in contractile markers which are required to maintain the healthy vascular tone of brain arterioles. During vessel injury, VSMC phenotype switching is induced by various pro-inflammatory cytokines (i.e., interleukins and TNFα) (Tyrrell and Goldstein, 2021) or growth factors (i.e., platelet-derived growth factors [PDGFs] and fibroblast growth factors) (Claesson-Welsh, 1996; Kendrick et al., 2011). Interestingly, synthetic VSMC-secreted proteins are associated with known neurodegenerative markers, including the production of Coffilin-1, matrix metallopeptidase 9 (MMP9), and proinflammatory signals, such as CD68, IL-6, VCAM-1, ICAM-1, and MCP-1 (Lino Cardenas et al., 2019; Li et al., 2020a, 2020b). Therefore, there is a critical need to resolve the causal role of VSMCs and vascular dysfunction underlying AD progression. In this study, we show that dysfunctional VSMCs can contribute to the AD development through the production of neuroinflammatory molecules including CD68, MMP9, and IL-6R. We also show that VSMCs can generate elevated quantities of Tau protein as well induce its hyperphosphorylation at multiple sites, further implicating VSMCs in the initiation and progression of AD pathogenesis.

RESULTS

Dysfunctional VSMCs contribute to brain inflammation and Tau hyperphosphorylation

The role of VSMCs in neuroinflammation and Tau hyperphosphorylation is poorly understood. Thus, we performed a transcriptomics analysis of previously described markers of a VSMC phenotypic state from brains of healthy individuals and patients with AD (Bennett et al., 2014). Interestingly, brains of patients with AD exhibited an upregulation of synthetic VSMC genes including *GJA*, *S100A4*, *CALD1*, and *PDGFR-β* (known to be a potent inducer of VSMC dysfunction). Remarkably, genes that associated with vascular-related diseases including *LTBP3* (aortic dissection) (Guo et al., 2018), *PRKG1* (thoracic aortic aneurysm) (Isselbacher et al., 2016), and *TLN1* (coronary atherosclerosis) (Li et al., 2020a, 2020b) were also found to be upregulated in brains of patients with AD (Figure 1A and Table S1). In contrast, expression of contractile VSMC genes was almost undetectable in brains of patients with AD indicating loss of healthy VSMC phenotype, consistent with previous observations in other forms of VSMC-related diseases (Frismantiene et al., 2018; Owens et al., 2004; Mack, 2011). We then validated these observations in a second publicly available transcriptome data set across 7 different brain regions using a bulk RNA-seq data set (Table S2) (Wan et al., 2020). Like our initial RNA-seq, analysis also showed that brains of patients with AD had increased levels of PDGFR-β that inversely correlated with SM22α (*TAGLN*). To investigate the role of VSMC dysfunction in AD, we evaluated the levels of contractile proteins (SM22α) in arterioles from brains of the humanized animal model of tauopathy and AD, the 3xTg-AD mice at 44 weeks (Oddo et al., 2003).

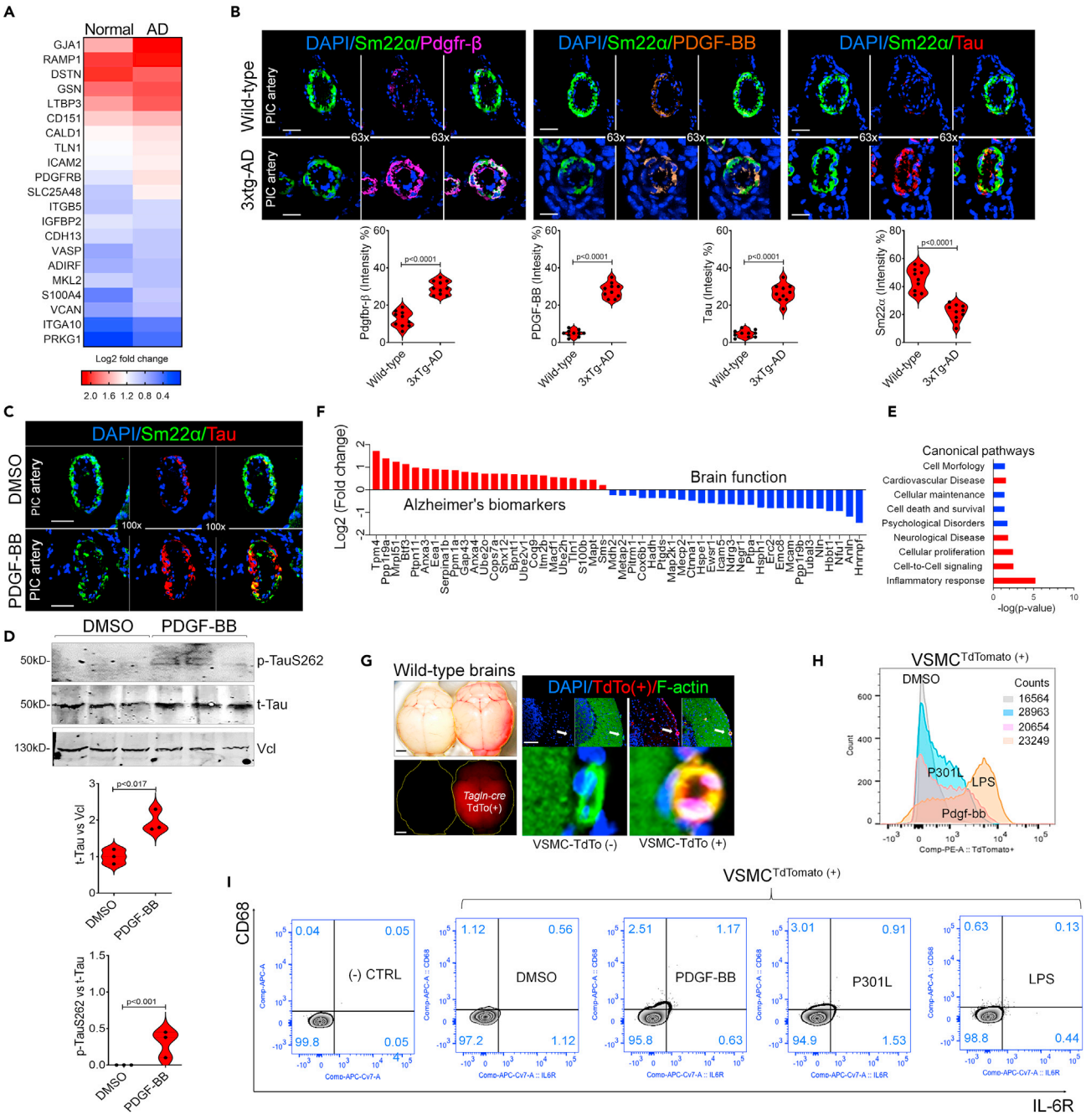

Figure 1. VSMC dysfunction contributes to brain inflammation and Tau hyperphosphorylation

(A) Heatmap of 21 VSMC genes differentially expressed (DEG) from the dorsolateral prefrontal cortex of postmortem brains of non-demented control individuals (n = 151) and patients with AD (n = 257). The scale bar indicates log2 fold change in expression determined from the limma R package.

(B) Immunofluorescence staining of coronal sections (8 μm thickness) of the mid-brain from wild-type (n = 5) and 3xTg-AD (n = 5) mice at 44 wks of age. Right image shows staining of posterior inferior cerebral arteries (PICA) at 63 X magnification. The images in wild type shows negligible amount of Pdgfr-β as compared to arterioles from 3xTg-AD mice which showed increased expression of Pdgfr-β colocalizing with Sm22a (VSMC marker). Middle image shows increased levels of PDGF-BB in PIC arteries in 3xTg-AD mice. Left image shows elevated levels of Tau protein in PIC arteries. The quantification of Tau expression was calculated as intensity % (n = 2 slides per brain, mean ± SEM, $p < 0.0001$) in the PICA artery. Respectively, compared to the corresponding control, it is determined by one-sample t test. Scale bars: 50 μm.

(C) Immunofluorescence staining of wild-type brains treated with PDGF-BB *ex vivo* (n = 3). The image demonstrates accumulation of Tau protein (Red) and downregulation of Sm22α (green) in 3xTg-AD arterioles. Scale bars: 80 μm.

Figure 1. *Continued*

(D) Western blot analysis of phospho-Tau-S262 and total Tau in brain lysates treated with PDGF-BB or DMSO *ex vivo*. The quantification of Total-Tau/VCL was calculated as mean ± SEM $p < 0.017$ (n = 3) and of phospho-Tau-S262/t-Tau levels was calculated as mean ± SEM, $p < 0.0001$ (n = 3). Respectively, compared to the corresponding control, it is determined by one-sample t test.

(E) Proteomics signature of AD-associated proteins expressed by wild-type brains treated with PDGF-BB *ex vivo* (n = 3). Scale bar indicates log2 fold change in expression of proteins.

(F) Ingenuity pathway analysis (IPA) of biological pathways impacted by proteomics changes in wild-type brains treated with PDGF-BB *ex vivo*. The scale bar represents log(p value) fold change.

(G) Generation of genetically labeled VSMC expressing red TdTomato under the control of *Tagln*-cre driver. Coronal section of frontal cortex (10 X magnification tile scan, scale bars: 20 μm.) shows arterioles (M3) TdTomato positive in red and F-actin in green.

(H) Representative proliferation histogram showing numbers of $VSMC^{TdTomanto}$ from wild-type brains under AD-like conditions, PDGF-BB (n = 3), Tau^{P301L} (n = 3), LPS (n = 3), or DMSO (n = 3), treated *ex vivo*. The y axis represents cell counts and x axis represents PE-A: TdTomato.

(I) Flow cytometry analysis of sorted $VSMC^{TdTomanto}$ from wild-type brains under AD-like conditions, PDGF-BB (n = 3), Tau^{P301L} (n = 3), LPS (n = 3), or DMSO (n = 3), treated *ex vivo*. Cells were gated on PE and CD68-positive (y axis) and IL-6R-positive (x axis) populations were determined.

Notably, we found that cortical (M3) and posterior inferior cerebellar arterioles had abnormal wall thickness with lower levels of Sm22α, which was associated with increased levels of PDGFR-β and its high affinity ligand, the platelet-derived growth factor BB (PDGF-BB) (Figure 1B). Moreover, 3xTg-AD brain arterioles contained high levels of Tau protein colocalizing especially with VSMCs as assessed by immunofluorescence analysis (Figure 1B). We then investigated whether dysfunctional VSMCs can contributes to neuroinflammation and thus treated healthy mouse brains *ex vivo* with PDGF-BB to induce VSMC phenotypic switching. After 48 hrs of incubation, the treated brains showed high levels of Tau protein in arterioles (Figure 1C) and CD68, a marker of neuroinflammation (Figure S1A). Further, western blot and quantitative proteomics analysis of PDGF-BB *ex vivo* treated brains showed hyperphosphorylation of Tau S262 (Figure 1D) and upregulation of multiple known molecular pathways associated with AD, including altered cell-to-cell signaling, neurological diseases, cell proliferation, and neuroinflammation (Figures 1F–1E).

The activation of neuroinflammatory signals observed in the proteomic analysis could come from other cell types in PDGF-BB-treated brains such microglial cells. We isolated the inflammatory contribution of VSMCs by using mouse brains with genetically labeled VSMCs that expressed a red fluorescent protein (TdTomato) under the control of the *Tagln-cre* (Sm22α) promoter (Figure 1G). To mimic AD conditions, we used 3 *in vitro* models of neuroinflammation (PDGF-BB, mutant Tau^{P301L}, and LPS). Flow cytometry analysis of sorted $VSMC^{TdTomato}$ from brains under AD-like conditions revealed that VSMCs adopt a proliferative (Figure 1H) and pro-inflammatory phenotype by expressing significant levels of CD68 and IL-6R as compared to DMSO controls (Figure 1I). Our results demonstrate that the mutant Tau^{P301L} model had the highest proportion of CD68 and IL-6R positive cells, followed by PDGF-BB treatment. In contrast, LPS treatment induced the lowest expression of both proinflammatory markers indicating a strong association between dysfunctional VSMCs and neurotoxicity rather than the activation of inflammatory pathways by LPS. Immunofluorescence staining analysis of brain arterioles from the 3xtg-AD mice also showed increased levels of CD68 within VSMCs (Figure S1B). Collectively, these findings demonstrate that dysfunctional VSMCs may play a critical role in neuroinflammation.

Morphological and phenotypic changes of VSMCs under AD-like conditions *in vitro*

To further investigate the contribution of dysfunctional VSMCs in AD, we used primary human VSMCs from neural crest lineage (Steinbach and Husain, 2016) which were treated with PDGF-BB, mutant Tau^{P301L}, and LPS. Under these conditions, VSMCs showed dramatic changes in their cytoskeleton morphology characterized by the formation of dendritic-like phenotype (lamellipodium) and loss of polarized cytoskeleton microfilaments (F-actin) (Figure 2A, top panel) which associated with increased Tau and MMP9 proteins levels (Figure 2A, lower panel). Consistent with these changes, there was a significant downregulation of contractile genes including *TAGLN* (SM22α), *LRP1*, and *CNN1*, especially in PDGF-BB and P301L conditions. This was inversely correlated with upregulation of synthetic and inflammatory genes such as *MMP9*, *GJA1*, *COL1A1*, *TNFα*, *IL-6*, *LGALS3*, and *CD68* genes (Figure 2B). Like our *ex vivo* results, flow cytometry analyses show that human VSMCs express inflammatory markers (CD68 and IL-6R) in PDGF-BB and Tau^{P301L} conditions but not with LPS treatment (Figure 2C), indicating that VSMCs undergo transdifferentiation to adopt a secretory and pro-inflammatory phenotype in response to neurotoxin stimuli.

Chronic inflammation has been shown to trigger microglial activation in AD (Navarro et al., 2018; Hansen et al., 2018). We also investigated the response of microglial cells to secretory VSMCs using a wound

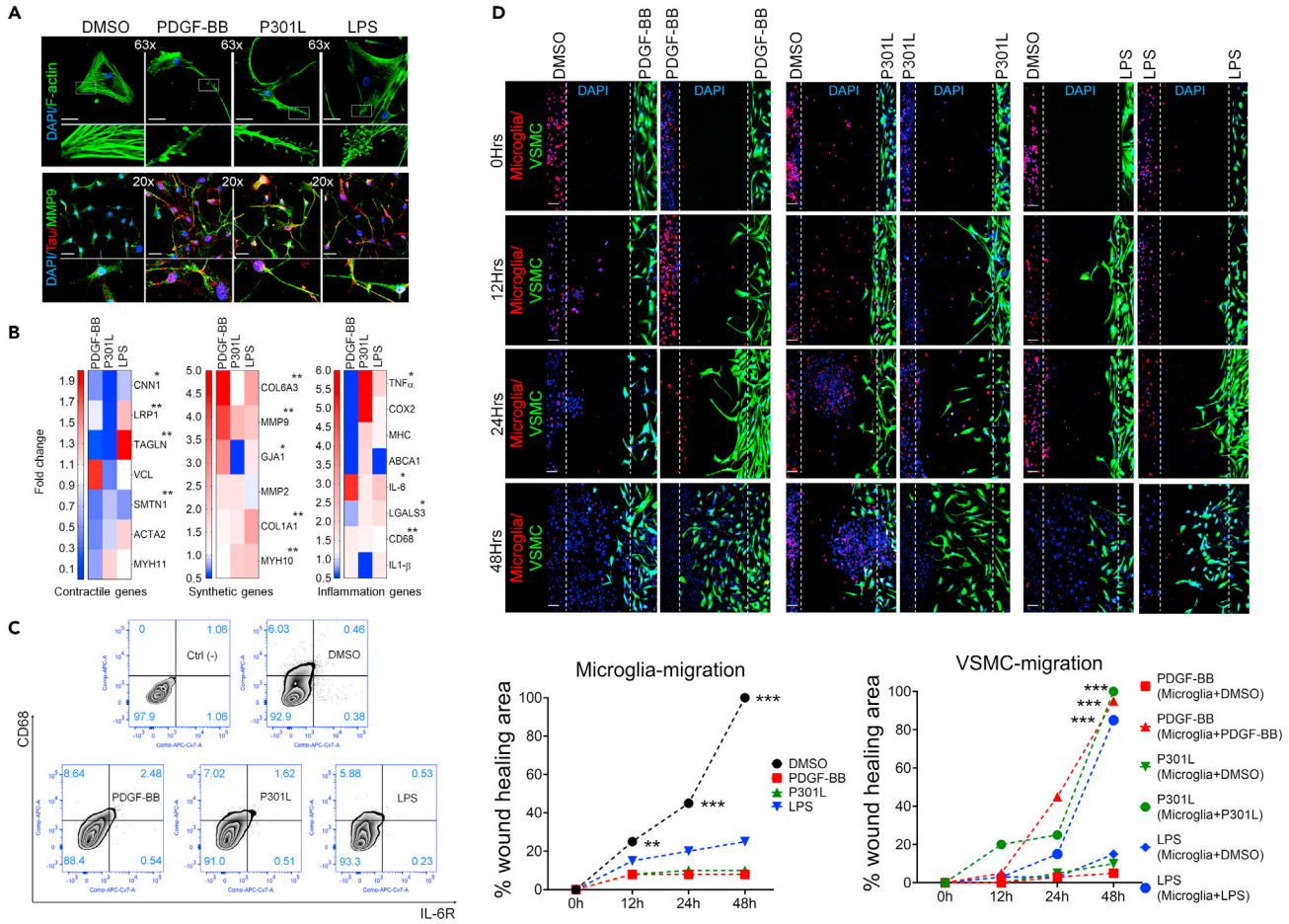

Figure 2. Phenotypic changes of VSMCs under AD-like conditions *in vitro*

(A) Immunofluorescence staining of primary human VSMCs stimulated with PDGF-BB, Tau^{P301L}, LPS, or DMSO for 72 hrs. Top image shows morphological changes in the cytoskeleton (F-actin, green), scale bars: 50 μm. Lower image shows increased Tau (red) and MMP9 (green) expression in VSMCs under AD-like conditions. Scale bars: 30 μm.

(B) Heatmap of mRNA expression of VSMCs under AD-like conditions versus control group (DMSO). Left image shows classic VSMC-contractile markers. Middle image shows VSMC synthetic makers, and right image shows inflammatory markers. Red indicates upregulated genes, white indicates no significant change, and blue indicates downregulated genes. *$p < 0.05$, **$p < 0.01$, ***$p < 0.001$ level of significance in genes upregulated as compared to control (DMSO). Respectively, compared to the corresponding control, it is determined by one-way analysis of variance (ANOVA).

(C) Flow cytometry analysis of CD68 and IL-6R expression in VSMCs under AD-like conditions.

(D) Would healing assay of co-cultured human VSMC and microglia cells. Microglia were labeled with CellTracker Deep Red Dye and DAPI nuclear stain. VSMCs were labeled with CellTracker Green Dye. The migratory activity of VSMCs and microglia were observed at 0, 12, 24, and 48 hr and quantified as the percentage wound healing area occupied by cells. Scale bars: 30 μm. *$p < 0.05$, **$p < 0.01$, ***$p < 0.001$ as compared to controls. Respectively, compared to the corresponding control, it is determined by one-sample t test.

healing assay. Under AD-like conditions, VSMCs enhanced the migratory ability of healthy microglia which seemed to have a propensity to inhibit the migratory properties of VSMCs treated with PDGF-BB, mutant Tau^{P301L}, or LPS (Figure 2D). However, when both cell types were incubated under AD-like conditions, microglia cells lose their ability to migrate while dysfunctional VSMCs displayed higher proliferation and migration activities indicating that microenvironments in AD brain may facilitate the proliferative and neuroinflammatory phenotype of VSMCs, thereby accelerating neurotoxicity in AD brains.

Dysfunctional VSMCs induce AD-associated microglial phenotype

To determine if dysfunctional VSMCs were able to activate microglial cells, we performed an invasion assay and co-culture experimentations to quantify the migratory potential of microglia in response to inflammatory signals from VSMCs treated with PDGF-BB, Tau^{P301L}, and LPS. To achieve this goal, we first labeled

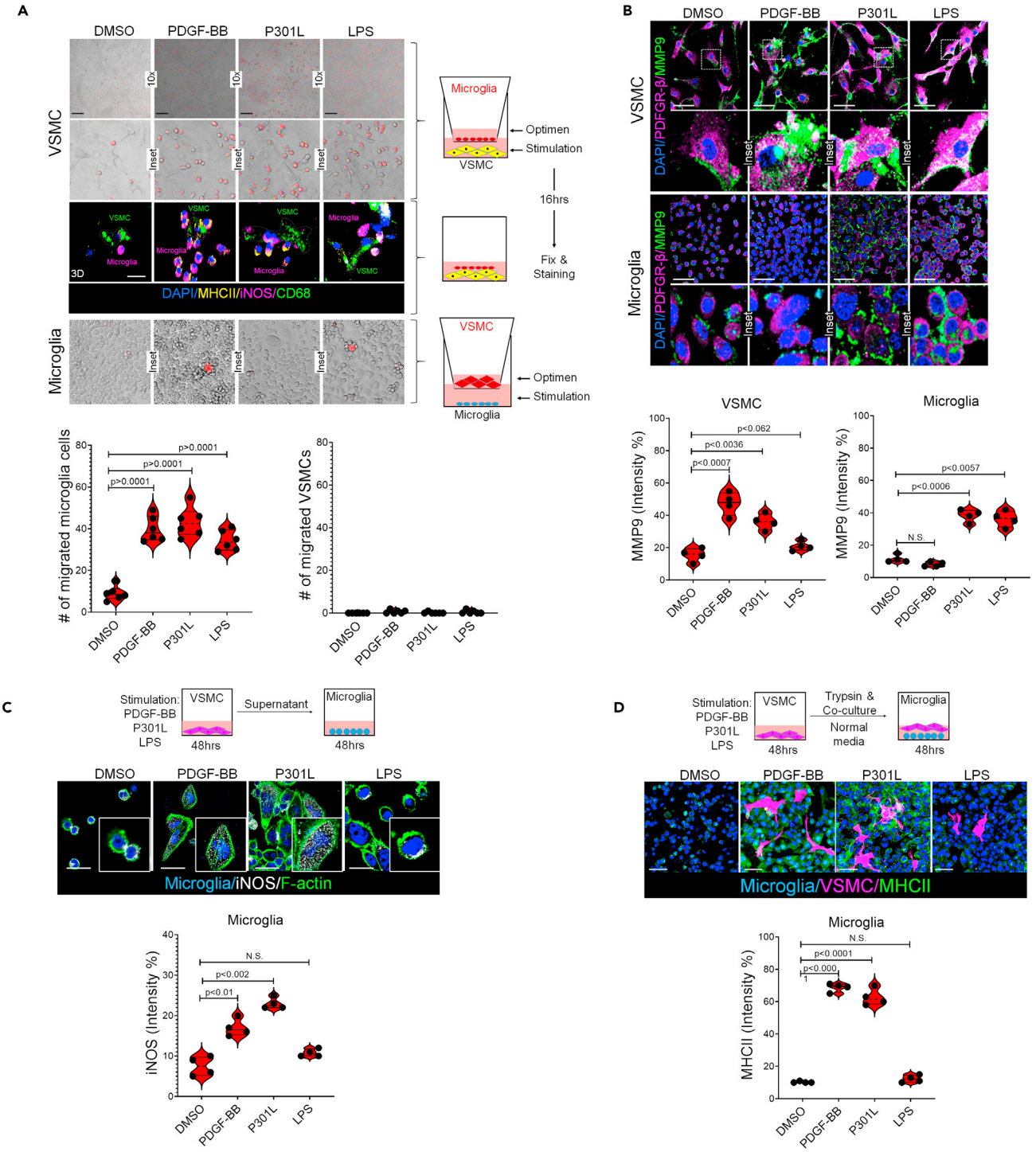

Figure 3. Dysfunctional VSMCs induce AD-associated microglial activation phenotype

(A) Trans-well invasion assay. Upper image, VSMCs (at bottom) were treated with PDGF-BB, Tau^{P301L}, LPS, or DMSO for 72 hrs, and then, the top chamber was introduced with microglia (red) under normal conditions for 16 hrs. Scale bars: 20 μm. Middle image, the immunostaining showed CD68-positive VSMCs (green) and MHC-II (yellow) and iNOS-positive (magenta) microglia displaying activation, scale bars: 50 μm. The lower panel shows that microglia under AD-like conditions did not promote trans-well migration of healthy VSMCs.

(B) Immunofluorescence staining show inflammatory marker expressed by VSMCs and microglia under AD-like conditions including MMP9 (green) and PDGFR-B (magenta), at 40 X magnification, scale bars: 30 μm.

Figure 3. *Continued*

(C) Immunofluorescence staining shows microglia activation after incubation with supernatant from dysfunctional VSMCs. Activated microglial were characterized by morphologic changes and elevated expression of iNOS, at 63 X magnification, scale bars: 50 μm.

(D) Co-culture assay shows that VSMCs (magenta) pre-treated with PDGF-BB, Tau^{P301L}, LPS, or DMSO for 72 hrs induced microglia (blue) activation as assessed by immunofluorescence staining of MHCII, at 40 X magnification, scale bars: 30 μm.

microglia cells with a membrane-binding red fluorophore in normal media, and in parallel, VSMCs were plated under AD-like conditions. Remarkably, microglial cells migrated significantly toward to stimulated VSMCs (Figure 3A, top panel). Immunofluorescence analysis of pro-inflammatory markers for activated microglia (M1 microglia) such as MHC-II and iNOS demonstrated that, under AD-like conditions, VSMCs can induce the activation of microglia potentially through a paracrine communication. Interestingly, confocal analyses revealed CD68 colocalization with SM22α, with evidence of microglia physically interacting with VSMCs, analogous to previously reported microglia-neuron interactions in the brain (Pósfai et al., 2019) (Figure 3A, middle panel and S2A). In contrast, pre-treatment of microglia cells with all three AD-like neurotoxins failed to promote the migration of healthy VSMCs (Figure 3A, Lower panel). Immunostaining showed increased levels of MMP9 and PDGFR-β in VSMCs under AD-like conditions. However, PDGF-BB treatment failed to induce MMP9 expression in microglial cells, supporting the notion of a paracrine VSMC-mediated activation of microglial cells in brains of patients with AD (Figure 3B). To support this idea, we performed a second experiment using the supernatant of VSMCs pre-treated with all 3 neurotoxins and determined if secreted inflammatory molecules (e.g. CD68) can promote the activation of healthy microglia. Immunofluorescence analysis showed that incubation of microglia cells with supernatants from VSMCs treated with PDGF-BB or Tau^{P301L} was sufficient to promote morphologic and phenotypic changes corresponding to activated microglia associated with brain neuroinflammation in patients with AD (Figure 3C) (Leng at al., 2020). Then, we co-cultured dysfunctional VSMCs with healthy microglia cells under normal conditions. And observed that only VSMCs pre-treated with PDGF-BB or Tau^{P301L} induced expression of the classic M1 microglial marker (MHC-II) but LPS-treated VSMCs failed to activate microglia, indicating that the phenotypic switching of VSMCs under AD-like conditions is required to trigger their neurotoxic behavior (Figure 3D). Thus, dysfunctional VSMCs show a paracrine mechanism by which they can activate the AD-associated microglia phenotype and thus contribute to brain neuroinflammation.

Dysfunctional VSMCs induce Tau hyperphosphorylation and an *in silico* analysis of mutant Tau proteins

Hyperphosphorylated Tau is a histopathological hallmark of AD and related tauopathies. To further examine the impact of VSMC dysfunction in tau pathology in a neurodegenerative context, we analyzed multiple Tau phosphorylation sites previously associated with early and late onset of symptoms in AD. Importantly, immunoblot analysis of total lysates showed that dysfunctional VSMCs can produce high levels of both total and phosphorylated Tau. Indeed, VSMCs treated with PDGF-BB and Tau^{P301L} promoted predominately the hyperphosphorylation of the S262 residue and other residues including Y18 and T205. These PTMs were associated with upregulation of Cofilin-1, a marker of proliferative VSMCs (San et al., 2008) which has recently been implicated in the pathogenesis of AD (Kang and Woo, 2019) (Figure 4A). Intriguingly, P301L mutation induced the hyperphosphorylation of residues that were not involved with the environment of the R2-R3 domains. Thus, we sought to use an *in silico* approach to provide insights into the molecular and structural impact of mutations in the Tau protein associated with neurodegenerative diseases (described in STAR Methods). Therefore, we performed an *in silico* study using molecular dynamics simulations (MDSs) (Table S3). By using the Tau full-length 2N4R sequences (441 aa), we built the 3D structure of the protein (Figures S3A and S3B; Video S1). Then, based on this 3D model, Tau^{P301S} and Tau^{P301L} were built performing 301 site direct mutagenesis using UCSF Chimera software (Pettersen et al., 2004), allowing local structural relaxation to avoid steric residue clashes (Figures 4B and S3C). Tau isoforms are considered intrinsically disordered proteins; there is evidence that, in solution, they can adopt multiple globular structures (Popov et al., 2019). Thus, we sought to analyze all three Tau proteins with 500 ns of MDSs to stabilize the physical motions of atoms in the Tau proteins to mimic physiological conditions. Importantly, the residue 301 is located at the microtubule-binding repeat domains R2 and R3 (MTBRs) where the assembly and stabilization of axonal connections occurs at the neuronal cell body (Figures S4A–S4E). Even though all three proteins fold toward a globular structure, the folding was remarkably different for the Tau protein with a proline-to-leucine substitution compared to the proline-to-serine substitution. While looking at the global surface of the Tau^{P301L}, we observed a decrease in the solvent-

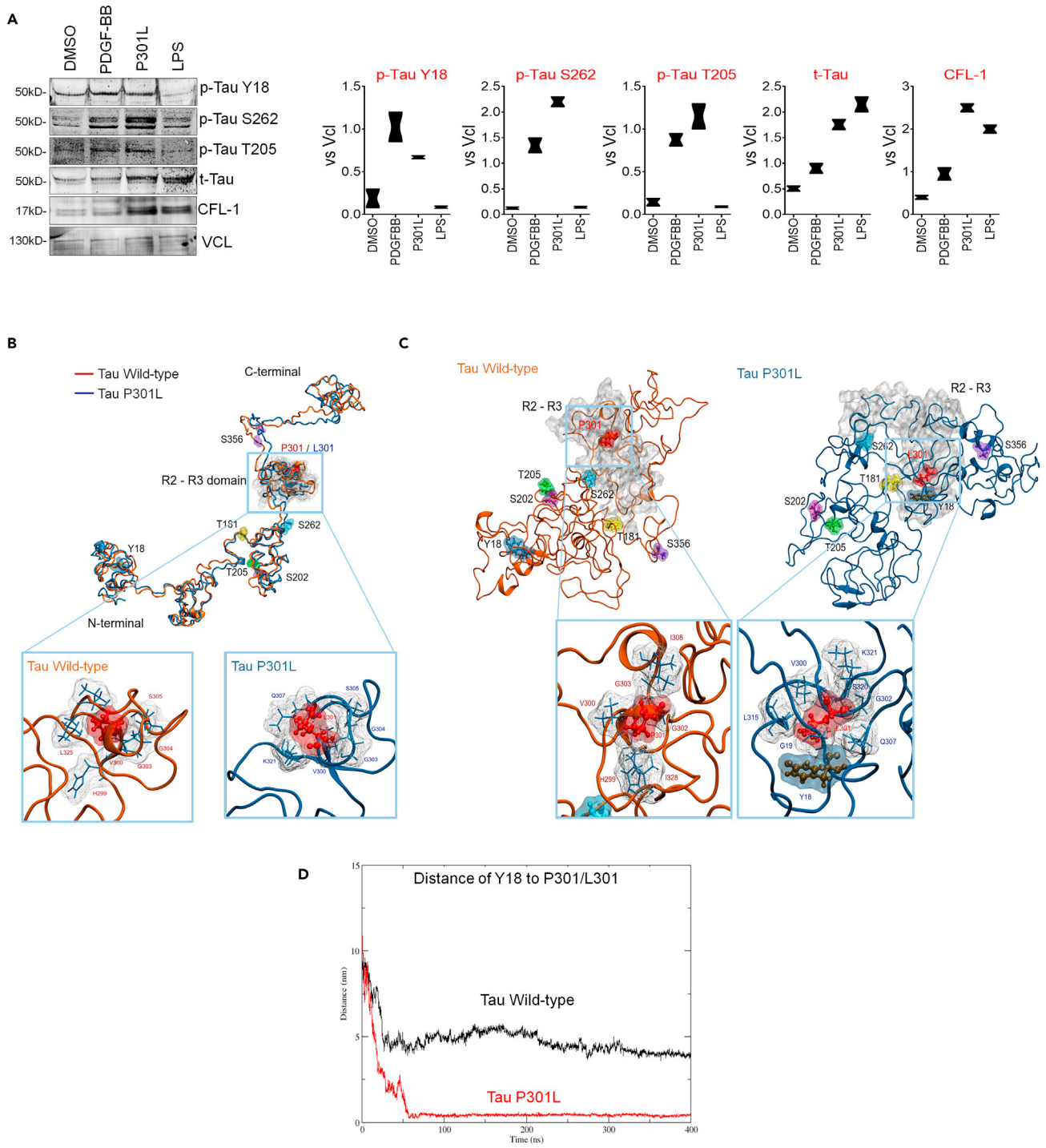

Figure 4. Dysfunctional VSMCs induce Tau hyperphosphorylation and an *in silico* analysis of mutant Tau proteins

(A) Representative western blots shows levels of total Tau (t-Tau) and multiple phosphorylate Tau residues (p-tau-Y18, p-tau-S262, p-tau-T205) from total lysates of VSMCs under AD-like conditions. CFL-1 (Coflin-1, a proliferative marker of VSMC). VCL was used as loading internal control.

(B and C) *In silico* analysis of the WT and mutant Tau^{P301L} proteins.

(D) Plot of distance (nm) vs time of the Y18 residue and R2-R3 domains after 500 ns of molecular dynamics simulations (MDSs) shows a significant reduction between the Y18 residue and the L301 mutant residue.

accessible surface area (SASA) from 360 nm^2 to 240.31 nm^2. The MTBR domain showed a significant increase in the SASA (7%), potentially exposing a greater area of interaction and thus creating a predisposition to PTM including phosphorylation of multiple residues (Table S4). Another important consequence of the proline-to-leucine substitution was observed on the electrostatic potential surfaces at the MTBRs. All three proteins show nucleophilic and hydrophobic interactions. However, the R3-R4 domains of the Tau^{P301L} adopt an additional negative electrostatic pattern creating a more promiscuous Tau protein which may be more prone to interact with multiple Tau-protein kinases and ligands (Figures S5A–S5C). To achieve these conformational changes, the proline-to-leucine substitution induces loss of residue contacts at H299, V300, G303, G304, S305, V309, and L325 and creates uncommon interactions with residues at Q307, K321, and N-terminal regions (Figures 4B and 4C, S4A and S4C–S4E). Remarkably, the misfolding of the Tau^{P301L} protein reduced the distance of the Y18 residue toward to the MTBRs where the P301L substitution occurs (Figures 4D and S6A–S6E). In this context, the S262 residue showed the largest area of exposure to the solvent and thereby augmented its capability to interact with Tau-protein kinases (Figures S7A and S7B). Similarly, multiple Tau residues previously associated with brain neurodegeneration were relocated at the proximity of the proline-to-leucine substitution and augmented their ability to PTMs (Figure 4C and Video S2). Thus, Tau misfolding is associated with hyperphosphorylation and strongly supports the notion that dysfunctional VSMCs can induce conformational changes in Tau protein and neurotoxicity previously implicated in tauopathies including AD.

VSMCs adopt an inflammatory phenotype in an age-dependent manner in Alzheimer disease models

The use of transgenic mouse models of AD has helped to understand the disease mechanisms and provided opportunities for developing potential therapies. Thus, we performed an in-depth analysis of brain arterioles in two well-characterized mouse models of tauopathies and AD such as the 3xtg-AD and 5xFAD mice at 13, 27, and 44 weeks of age. Immunofluorescence analysis demonstrated that loss of contractile proteins (Sm22α) in brain arterioles correlates with an increased production of Tau within VSMCs in an age-dependent manner (Figures 5A and 5B). Interestingly, we observed that Tau accumulation in brain arterioles of the 3xtg-AD mice began at 13 weeks of age indicating the early involvement of VSMCs in brain inflammation even before the formation of plaques and neuronal loss. The increase in Tau protein was accentuated at 27 and 44 weeks of age in both animal models of AD when the production of neurofibrillary tangles and cognitive impairment are well established. Regarding the expression of CD68, we observed that its production began to increase from 27 weeks of age, preceding Tau accumulation suggesting that the secretion of inflammatory bodies from the brain arterioles may contribute to the acceleration of cognitive decline. These data may help to inform the specific pathologic role of dysfunctional VSMCs in neuroinflammation and clear temporal relationship between the cerebrovascular unit and the pathogenesis of AD.

DISCUSSION

Vascular dysfunction is a well-established clinical aspect of AD, with subtle changes in microvasculature of the brain manifesting at the onset of clinical symptoms (Govindpani et al., 2019; Arvanitakis et al., 2016). However, the precise role of VSMCs in the pathogenesis of AD remains unclear. The NVU is primarily composed of endothelial cells, pericytes, astrocytes, and VSMCs (Zlokovic, 2011). Given the inherent phenotypic plasticity of VSMCs, they readily switch from normal contractile to synthetic phenotypes in response to a variety of environmental stimuli, including inflammatory cytokines, genetic mutations, or chemical compounds. Previous neuropathological studies of AD autopsies showed that 80% of patients with AD without vascular dementia developed abnormal vascular features, including multiple micro-infarcts, lacunes, cerebral micro-bleeds indicative of intracranial atherosclerosis, perivascular spacing, and cerebral amyloid angiopathy (Toledo et al., 2013). Together, these observations support the concept that cerebrovascular dysfunction is a prominent pathological feature of AD and that the NVU is a central catalyst of AD initiation and progression.

Our findings point toward the contribution of dysfunctional VSMCs in the development of neuroinflammation and AD progression. In this study, downregulation of contractile genes critical for the homeostasis of brain arterioles was tightly linked to the production of neuroinflammatory markers such as MMP9, CD68, and IL-6. Moreover, transdifferentiated VSMCs can produce high levels of total and hyperphosphorylated Tau protein. Remarkably, under AD-like conditions, VSMCs promoted hyperphosphorylation of Tau-T205 which has been associated with early neurological decline in patients with AD, further illuminating the

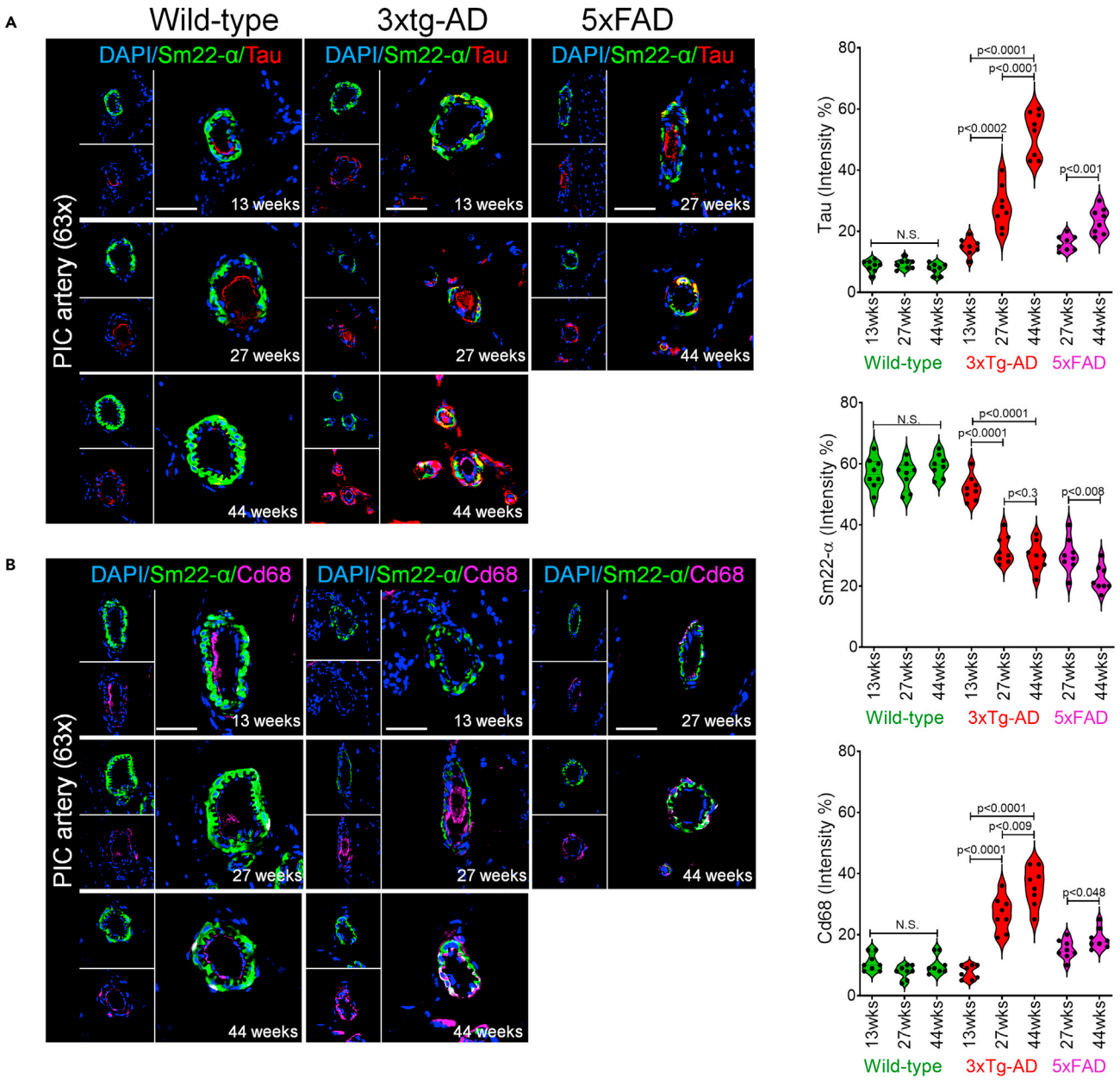

Figure 5. Age-dependent accumulation of Tau and Cd68 protein in brain arterioles of the 3xtg-AD and 5xFAD transgenic mice

(A and B) Immunofluorescence staining of coronal sections (8-μm thickness) of the mid-brain from wild-type (n = 4), 3xTg-AD (n = 4), and 5xFAD mice at 13, 27, and 44 wks of age. (A) shows staining of Tau (red) and Sm22α (green) in posterior inferior cerebral arteries (PICA) at 63 X magnification. (B) shows staining of Cd68 (magenta) and Sm22α (green) in posterior inferior cerebral arteries (PICA) at 63 X magnification. (Two slides per brain, mean ± SEM, $p < 0.0001$) in the PICA artery. Respectively, compared to the corresponding control, it is determined by one-way ANOVA. Scale bars: 80 μm.

contribution of VSMCs in the initiation of clinical symptoms. We found that brain arterioles of 3xTg-AD mice contained high levels of PDGFBB (platelet-derived growth factor-BB), which is a well-known inducer of VSMC transdifferentiation through a potent mitogenic activity by inhibiting expression of contractile genes such as αSMA (*ACTA2*), SM22α (*TAGLN*), LRP1, and CNN1 (Calponin) (Tallquist and Kazlauskas, 2004; Salabei et al., 2013). Furthermore, MMP proteins known to be associated with other VSMC-related diseases including aortic aneurysm, vascular calcification, and vascular stenosis were also found elevated in the post-mortem brain tissue of patients with AD. In agreement with our work, elevated MMP proteins in VSMCs under AD-like conditions coincided with downregulation of SM22α, which is known to be a negative regulator

of MMP9 (Nair et al., 2006) indicating the negative feedback regulation of neuroinflammatory molecules due to loss of VSMC contractile phenotype. Similarly, downregulation of LRP1 in VSMCs was observed in AD-like conditions and may impact Aβ clearance leading to Aβ accumulation and plaque formation during diseases state (DeSimone et al., 2017; Kanekiyo et al., 2012; Nelson et al., 2017). Along these lines, microglia cells have an increased phagocytic response to Aβ and are known effectors of Aβ clearance in the brain (Lopes et al., 2008; Streit et al., 2009). However, during AD, microglia adopt reactive states characterized by both morphological and functional changes including increased expression of iNOS and MHC-II and other acute inflammatory molecules (Zabel et al., 2013). Our *in vitro* assays demonstrated the potential of dysfunctional VSMCs to trigger AD-associated microglial phenotypes. These changes were more remarkable in PDGFBB and Tau^{P301L} conditions, further supporting the contribution of unhealthy VSMCs in promoting AD-related pathology features and neurodegeneration.

Some forms of genetically triggered neurodegenerative diseases such as Tau^{P301L} protein promote neurofibrillary deposits (Kawasaki and Tate, 2020). Tau hyperphosphorylation may promote self-aggregation and subsequent fibrillization (Eschmann et al., 2017; Berendsen and Hayward, 2000). Our *in silico* analysis of the 3D structures of wild-type and Tau^{P301L} proteins demonstrates that changes in the amino acid sequence could have a dramatic impact on the conformational structure and misfolding, leading to the phosphorylation of multiple residues via rearrangement of key amino acids (e.g. Y18, T181, S202, T205, S262, and S356) involved in AD progression. In agreement with our *in silico* analysis, we found that dysfunctional VSMCs can induce Tau misfolding and promote its hyperphosphorylation. In addition, our *in vivo* studies reveal that brain arterioles contained significant levels of Tau protein and inflammatory markers co-localizing with VSMCs in 3xTg-AD mice. Additionally, we uncovered that Tau protein levels and inflammatory signal were relative to the age of the 3xTg-AD and 5xFD mice, indicating that the vascular tissue may play a pathological role in the development of the disease as early as before the outcome of clinical symptoms.

Overall, this study demonstrates the pivotal role of VSMC dysfunction in AD development and progression. It has refined our understanding of the contributory role of the NVU and the direct contribution of VSMC toward AD pathogenesis. While most AD studies have focused on neural and glial cells, this study extends the catalog of promoting factors in AD which promise to enable development of new therapeutic interventions and vascular-related biomarkers for early detection of the disease. In this context, recent studies have showed that targeting the vascular tissue with drugs such as Losartan, ACEi, or Captopril could help to improve memory and cognitive decline (Lee et al., 2020; Royea et al., 2020; Royea et al., 2020, 2020; Asraf et al., 2018; Rahimi et al., 2021). Therefore, this study supports the idea of VSMCs as promising therapeutic targets in AD.

Limitations of the study

In our current study, we have used *in vitro*, *in silico*, and *in vivo* tools to investigate the role of VSMCs in the pathogenesis of AD. Our findings provide new insights into how VSMC dysfunction contributes to neuroinflammation and Tau hyperphosphorylation. However, the involvement of amyloid-β deposits in the NVU has not been addressed in this study. We consider that further mechanistic studies are certainly needed to better understand the involvement of VSMCs in neurodegenerative diseases such as AD.

STAR★METHODS

Detailed methods are provided in the online version of this paper and include the following:

- KEY RESOURCES TABLE
- RESOURCE AVAILABILITY
  - Lead contact
  - Material availability
  - Data and code availability
- METHODS DETAILS
  - Human Alzheimer disease, vascular SMC gene expression analysis
  - Mouse lines
  - Cell lines for *in vitro* experiments
  - *Ex-vivo* experiments and AD-like models
  - Proteomic analysis

- Quantitative flow cytometry
- RNA extraction and qPCR analysis
- Wound healing assay
- Cell invasion assay and immunostaining
- Immunoblotting
- Computational details

- QUANTIFICATION AND STATISTICAL ANALYSIS

SUPPLEMENTAL INFORMATION

Supplemental information can be found online at https://doi.org/10.1016/j.isci.2021.102993.

ACKNOWLEDGMENTS

This research was funded by Consejo Nacional de Ciencia, Tecnología e Innovación Tecnológica de Perú (grant N°024-2019-Fondecyt-BM-INC.INV and CONCYTEC-FONDECYT- E038-01).

AUTHOR CONTRIBUTIONS

Conceptualization: C.L.L.C.; data curation: C.L.L.C., J.A.A.P., M.A.C.F., K.J.V.L., K.L.A.-F., and B.G.-V.; formal analysis: C.L.L.C., J.A.A.P., L.D.G.M., and R.N.M.; funding acquisition: C.L.L.C., K.J.V.L., and G.D.D.-C investigation: C.L.L.C., J.A.A.P., M.A.C.F., P.S., and C.L.M.; methodology: C.L.L.C., and J.A.A.P.; writing – review & editing: C.L.L.C., R.M., and M.E.L. All authors have read and agreed to the published version of the manuscript.

DECLARATION OF INTERESTS

The authors declare no competing interests.

Received: March 7, 2021
Revised: June 17, 2021
Accepted: August 13, 2021
Published: September 24, 2021

REFERENCES

Abraham, M.J., Murtola, T., Schulz, R., Páll, S., Smith, J.C., Hess, B., and Lindahl, E. (2015). GROMACS high performance molecular simulations through multi-level parallelism from laptops to supercomputers. SoftwareX *1-2*, 19–25. https://doi.org/10.1016/j.softx.2015.06.001.

Agarwal, P., Morris, M.C., and Barnes, L.L. (2020). Racial differences in dietary relations to cognitive decline and Alzheimer's disease risk: do we know enough? Front Hum. Neurosci. *14*, 359. https://doi.org/10.3389/fnhum.2020.00359.

Alzheimer's Association. (2018). 2018 Alzheimer's disease facts and figures. Alzheimers Dement *14*, 367–429. https://doi.org/10.1016/j.jalz.2018.02.001.

Arvanitakis, Z., Capuano, A.W., Leurgans, S.E., Bennett, D.A., and Schneider, J.A. (2016). Relation of cerebral vessel disease to Alzheimer's disease dementia and cognitive function in elderly people: a crosssectional study. Lancet Neurol. *15*, 934–943. https://doi.org/10.1016/S1474-4422(16)30029-1.

Asraf, K., Torika, N., Apte, R.N., and Fleisher-Berkovich, S. (2018). Microglial activation is modulated by captopril: in vitro and in vivo studies. Front Cell Neurosci *12*, 116. https://doi.org/10.3389/fncel.2018.00116.

Baker, N.A., Sept, D., Joseph, S., Holst, M.J., and McCammon, J.A. (2001). Electrostatics of nanosystems: application to microtubules and the ribosome. PNAS *98*, 10037–10041. https://doi.org/10.1073/pnas.181342398.

Barthélemy, N.R., Li, Y., Joseph-Mathurin, N., Gordon, B.A., Hassenstab, J., Benzinger, T.L.S., Buckles, V., Fagan, A.M., Perrin, R.J., Goate, A.M., et al. (2020). Dominantly inherited Alzheimer network. A soluble phosphorylated tau signature links tau, amyloid and the evolution of stages of dominantly inherited Alzheimer's disease. Nat. Med. *26*, 398–407. https://doi.org/10.1038/s41591-020-0781-z.

Barthélemy, N.R., Mallipeddi, N., Moiseyev, P., Sato, C., and Bateman, R.J. (2019). Tau phosphorylation rates measured by mass spectrometry differ in the intracellular brain vs. extracellular cerebrospinal fluid compartments and are differentially affected by Alzheimer's disease. Front Aging Neurosci. *11*, 121. https://doi.org/10.3389/fnagi.2019.00121.

Bennett, D.A., Yu, L., and De Jager, P.L. (2014). Building a pipeline to discover and validate novel therapeutic targets and lead compounds for Alzheimer's disease. Biochem. Pharmacol. *88*, 617–630. https://doi.org/10.1016/j.bcp.2014.01.037.

Berendsen, H., and Hayward, S. (2000). Collective protein dynamics in relation to function. Curr. Opin. Struct. Biol. *10*, 165–169. https://doi.org/10.1016/s0959-440x(00)00061-0.

Berendsen, H.J., Postma, J.V., van Gunsteren, W.F., DiNola, A.R.H.J., and Haak, J.R. (1984). Molecular dynamics with coupling to an external bath. J. Chem. Phys. *81*, 3684–3690. https://doi.org/10.1063/1.448118.

Brown, S.P., and Muchmore, S.W. (2009). Large-scale application of high-throughput molecular mechanics with Poisson−Boltzmann surface area for routine physics-based scoring of protein−ligand complexes. J. Med. Chem. *52* (10), 3159–3165. https://doi.org/10.1021/jm801444x.

Bussi, G., Donadio, D., and Parrinello, M. (2007). Canonical sampling through velocity rescaling. J. Chem. Phys. *126*, 014101. https://doi.org/10.1063/1.2408420.

Castro, P.R., Barbosa, A.S., Pereira, J.M., Ranfley, H., Felipetto, M., Gonçalves, C.A.X., Paiva, I.R., Berg, B.B., and Barcelos, L.S. (2018). Cellular and molecular heterogeneity associated with vessel formation processes. Biomed. Res. Int. *2018*, 6740408. https://doi.org/10.1155/2018/6740408.

Chan, K.Y., Wang, W., Wu, J.J., Liu, L., Theodoratou, E., Car, J., Middleton, L., Russ, T.C., Deary, I.J., Campbell, H., et al. (2013). Global

Health Epidemiology Reference Group (GHERG). Epidemiology of Alzheimer's disease and other forms of dementia in China, 1990–2010: a systematic review and analysis. Lancet *381*, 2016–2023. https://doi.org/10.1016/S0140-6736(13)60221-4.

Claesson-Welsh, L. (1996). Mechanism of action of platelet-derived growth factor. Int. J. Biochem. Cell Biol *28*, 373–385. https://doi.org/10.1016/1357-2725(95)00156-5.

De la Torre, J. (2018). The vascular hypothesis of Alzheimer's disease: a key to preclinical prediction of dementia using neuroimaging. J. Alzheimers Dis. *63*, 35–52. https://doi.org/10.3233/JAD-180004.

DeSimone, C.V., Graff-Radford, J., El-Harasis, M.A., Rabinstein, A.A., Asirvatham, S.J., and Holmes, D.R., Jr. (2017). Cerebral amyloid angiopathy: diagnosis, clinical implications, and management strategies in atrial fibrillation. J. Am. Coll. Cardiol. *70*, 1173–1182. https://doi.org/10.1016/j.jacc.2017.07.724.

Dolinsky, T.J., Nielsen, J.E., McCammon, J.A., and Baker, N.A. (2004). PDB2PQR: an automated pipeline for the setup of Poisson–Boltzmann electrostatics calculations. Nucleic Acids Res. *32*, W665–W667. https://doi.org/10.1093/nar/gkh381.

Dumanchin, C., Camuzat, A., Campion, D., Verpillat, P., Hannequin, D., Dubois, B., Saugier-Veber, P., Martin, C., Penet, C., Charbonnier, F., et al. (1998). Segregation of a missense mutation in the microtubule-associated protein tau gene with familial fronto-temporal dementia and parkinsonism. Hum. Mol. Genet. *7*, 1825–1829. https://doi.org/10.1093/hmg/7.11.1825.

Erkinjuntti, T., Román, G., Gauthier, S., Feldman, H., and Rockwood, K. (2004). Emerging therapies for vascular dementia and vascular cognitive impairment. Stroke *35*, 1010–1017. https://doi.org/10.1161/01.STR.0000120731.88236.33.

Eschmann, N.A., Georgieva, E.R., Ganguly, P., Borbat, P.P., Rappaport, M.D., Akdogan, Y., Freed, J.H., Shea, J.E., and Han, S. (2017). Signature of an aggregation-prone conformation of tau. Sci. Rep. *7*, 44739. https://doi.org/10.1038/srep44739.

Ewald, P.P. (1921). Die Berechnung optischer und elektrostatischer Gitterpotentiale. Annalen der physik *369*, 253–287. https://doi.org/10.1002/andp.19213690304.

Frismantiene, A., Philippova, M., Erne, P., and Resink, T.J. (2018). Smooth muscle cell-driven vascular diseases and molecular mechanisms of VSMC plasticity. Cell Signal *52*, 48–64. https://doi.org/10.1016/j.cellsig.2018.08.019.

Giménez-Llort, L., Arranz, L., Maté, I., De, la, and Fuente, M. (2008). Gender-specific neuroimmunoendocrine aging in a triple-transgenic 3xTg-AD mouse model for Alzheimer's disease and its relation with longevity. Neuroimmunomodulation *15*, 331–343. https://doi.org/10.1159/000156475.

Govindpani, K., McNamara, L.G., Smith, N.R., Vinnakota, C., Waldvogel, H.J., Faull, R.L., and Kwakowsky, A. (2019). Vascular dysfunction in Alzheimer's disease: a prelude to the pathological process or a consequence of it? J. Clin. Med. *8*, 651. https://doi.org/10.3390/jcm8050651.

Guo, D.C., Regalado, E.S., Pinard, A., Chen, J., Lee, K., Rigelsky, C., Zilberberg, L., Hostetler, E.M., Aldred, M., Wallace, S.E., Prakash, S.K., University of Washington Center for Mendelian Genomics, Leal, S.M., Bamshad, M.J., Nickerson, D.A., Natowicz, M., Rifkin, D.B., and Milewicz, D.M. (2018). LTBP3 pathogenic variants predispose individuals to thoracic aortic aneurysms and dissections. Am. J. Hum. Genet. *102*, 706–712. https://doi.org/10.1016/j.ajhg.2018.03.002.

Hansen, D.V., Hanson, J.E., and Sheng, M. (2018). Microglia in Alzheimer's disease. J. Cell Biol. *217*, 459–472. https://doi.org/10.1083/jcb.201709069.

Hess, B. (2008). P-LINCS: a parallel linear constraint solver for molecular simulation. J. Chem. Theor. Comput. *4*, 116–122. https://doi.org/10.1021/ct700200b.

Hockney, R.W., Goel, S.P., and Eastwood, J.W. (1974). Quiet high-resolution computer models of a plasma. J. Comput. Phys. *14*, 148–158. https://doi.org/10.1016/0021-9991(74)90010-2.

Humphrey, W., Dalke, A., and Schulten, K. (1996). VMD: visual molecular dynamics. J. Mol. Graphics. *14*, 33–38. https://doi.org/10.1016/0263-7855(96)00018-5.

Ibrahim, Y.M., Garimella, S.V., Prost, S.A., Wojcik, R., Norheim, R.V., Baker, E.S., Rusyn, I., and Smith, R.D. (2016). Development of an ion mobility spectrometry-orbitrap mass spectrometer platform. Anal Chem. *88*, 12152–12160. https://doi.org/10.1021/acs.analchem.6b03027.

Isselbacher, E.M., Lino Cardenas, C.L., and Lindsay, M.E. (2016). Hereditary influence in thoracic aortic aneurysm and dissection. Circulation *133*, 2516–2528. https://doi.org/10.1161/CIRCULATIONAHA.116.009762.

Janelidze, S., Berron, D., Smith, R., Strandberg, O., Proctor, N.K., Dage, J.L., Stomrud, E., Palmqvist, S., Mattsson-Carlgren, N., and Hansson, O. (2021). Associations of plasma phospho-tau217 levels with tau positron emission tomography in early Alzheimer disease. JAMA Neurol. *78*, 149–156. https://doi.org/10.1001/jamaneurol.2020.4201.

Jhoo, J.H., Kim, K.W., Huh, Y., Lee, S.B., Park, J.H., Lee, J.J., Choi, E.A., Han, C., Choo, I.H., Youn, J.C., et al. (2008). Prevalence of dementia and its subtypes in an elderly urban Korean population: results from the Korean Longitudinal Study on Health and Aging (KLoSHA). Dement Geriatr. Cogn. Disord. *26*, 270–276. https://doi.org/10.1159/000160960.

Jorgensen, W.L., and Madura, J.D. (1985). Temperature and size dependence for Monte Carlo simulations of TIP4P water. Mol. Phys. *56*, 1381–1392. https://doi.org/10.1080/00268978500103111.

Jorgensen, W.L., Maxwell, D.S., and Tirado-Rives, J. (1996). Development and testing of the OPLS all-atom force field on conformational energetics and properties of organic liquids. J. Am. Chem. Soc. *118*, 11225–11236. https://doi.org/10.1021/ja9621760.

Kalaria, R.N., Maestre, G.E., Arizaga, R., Friedland, R.P., Galasko, D., Hall, K., Luchsinger, J.A., Ogunniyi, A., Perry, E.K., Potocnik, F., et al. (2008). World Federation of Neurology Dementia Research Group. Alzheimer's disease and vascular dementia in developing countries: prevalence, management, and risk factors. Lancet Neurol. *7*, 812–826. https://doi.org/10.1016/S1474-4422(08)70169-8.

Kalaria, R.N. (2003). Comparison between Alzheimer's disease and vascular dementia: implications for treatment. Neurol. Res. *25*, 661–664. https://doi.org/10.1179/016164103101201968.

Kanekiyo, T., Liu, C.C., Shinohara, M., Li, J., and Bu, G. (2012). LRP1 in brain vascular smooth muscle cells mediates local clearance of Alzheimer's amyloid-β. J. Neurosci. *32*, 16458–16465. https://doi.org/10.1523/JNEUROSCI.3987-12.2012.

Kang, D.E., and Woo, J.A. (2019). Cofilin, a master node regulating cytoskeletal pathogenesis in Alzheimer's disease. J. Alzheimers Dis. *72*, S131–S144. PMID: 31594228. https://doi.org/10.3233/JAD-190585.

Kawasaki, R., and Tate, S.I. (2020). Impact of the hereditary P301L mutation on the correlated conformational dynamics of human tau protein revealed by the paramagnetic relaxation enhancement NMR experiments. Int. J. Mol. Sci. *21*, 3920. https://doi.org/10.3390/ijms21113920.

Kendrick, J., Cheung, A.K., Kaufman, J.S., Greene, T., Roberts, W.L., Smits, G., and Chonchol, M. (2011). HOST Investigators. FGF-23 associates with death, cardiovascular events, and initiation of chronic dialysis. J. Am. Soc. Nephrol. *22*, 1913–1922. https://doi.org/10.1681/ASN.2010121224.

Kim, S., Lee, M., and Choi, Y.K. (2020). The role of a neurovascular signaling pathway involving hypoxia-inducible factor and notch in the function of the central nervous system. Biomol. Ther. (Seoul) *28*, 45–57. https://doi.org/10.4062/biomolther.2019.119.

Kowalska, A. (2009). The genetics of dementias. Part 1: molecular basis of frontotemporal dementia and parkinsonism linked to chromosome 17. Postepy, Hig, Med. Dosw. *63*, 278–286.

Krämer, A., Green, J., Pollard, J., Jr., and Tugendreich, S. (2014). Causal analysis approaches in ingenuity pathway analysis. Bioinformatics *30*, 523–530. https://doi.org/10.1093/bioinformatics/btt703.

Kumari, R., and Kumar, R.; Open-Source Drug Discovery Consortium, Lynn, A (2014). g_mmpbsa A GROMACS tool for high-throughput MM-PBSA calculations. J. Chem. Inf. Model. *54*, 1951–1962. https://doi.org/10.1021/ci500020m.

Lamar, M., Boots, E.A., Arfanakis, K., Barnes, L.L., and Schneider, J.A. (2020). Common brain structural alterations associated with cardiovascular disease risk factors and Alzheimer's dementia: future directions and implications. Neuropsychol. Rev. *30*, 546–557. https://doi.org/10.1007/s11065-020-09460-6.

Lathuilière, A., Valdés, P., Papin, S., Cacquevel, M., Maclachlan, C., Knott, G.W., Muhs, A.,

Paganetti, P., and Schneider, B.L. (2017). Motifs in the tau protein that control binding to microtubules and aggregation determine pathological effects. Sci. Rep. *7*, 13556. https://doi.org/10.1038/s41598-017-13786-2.

Lee, S.H., Gomes, S.M., Ghalayini, J., Iliadi, K.G., and Boulianne, G.L. (2020). Angiotensin converting enzyme inhibitors and angiotensin receptor blockers rescue memory defects in drosophila-expressing Alzheimer's disease-related transgenes independently of the canonical renin angiotensin system. eNeuro *7*. ENEURO.0235-20. https://doi.org/10.1523/ENEURO.0235-20.2020.

Leszek, J., Małyszczak, K., Janicka, B., Kiejna, A., and Wiak, A. (2003). Total Tau in cerebrospinal fluid differentiates Alzheimer's disease from vascular dementia. Med. Sci. Monit. *9*, 484–488.

Li, T., Huang, Y., Cai, W., Chen, X., Men, X., Lu, T., Wu, A., and Lu, Z. (2020a). Age-related cerebral small vessel disease and inflammaging. Cell Death Dis *11*, 932. https://doi.org/10.1038/s41419-020-03137-x.

Li, Y., Gao, S., Han, Y., Song, L., Kong, Y., Jiao, Y., Huang, S., Du, J., and Li, Y. (2020b). Variants of focal adhesion scaffold genes cause thoracic aortic aneurysm. Circ. Res. *128*, 8–23. https://doi.org/10.1161/CIRCRESAHA.120.317361.

Lino Cardenas, C.L., Kessinger, C.W., Chou, E.L., Ghoshhajra, B., Yeri, A.S., Das, S., Weintraub, N.L., Malhotra, R., Jaffer, F.A., and Lindsay, M.E. (2019). HDAC9 complex inhibition improves smooth muscle-dependent stenotic vascular disease. JCI Insight *4*, e124706. https://doi.org/10.1172/jci.insight.124706.

Lobo, A., Launer, L.J., Fratiglioni, L., Andersen, K., Di Carlo, A., Breteler, M.M., Copeland, J.R., Dartigues, J.F., Jagger, C., Martinez-Lage, J., et al. (2000). Prevalence of dementia and major subtypes in Europe: a collaborative study of population-based cohorts. Neurologic diseases in the elderly research group. Neurology *54*, S4–S9.

Lopes, K.O., Sparks, D.L., and Streit, W.J. (2008). Microglial dystrophy in the aged and Alzheimer's disease brain is associated with ferritin immunoreactivity. Glia *56*, 1048–1060. https://doi.org/10.1002/glia.20678.

López-González, I., Garcia-Esparcia, P., Llorens, F., and Ferrer, I. (2016). Genetic and transcriptomic profiles of inflammation in neurodegenerative diseases: Alzheimer, Parkinson, Creutzfeldt-Jakob and Tauopathies. Int. J. Mol. Sci. *17*, 206. https://doi.org/10.3390/ijms17020206.

Mack, C.P. (2011). Signaling mechanisms that regulate smooth muscle cell differentiation. Arterioscler Thromb. Vasc. Biol. *31*, 1495–1505. https://doi.org/10.1161/ATVBAHA.110.221135.

Mok, S.S., Losic, D., Barrow, C.J., Turner, B.J., Masters, C.L., Martin, L.L., and Small, D.H. (2006). The beta-amyloid peptide of Alzheimer's disease decreases adhesion of vascular smooth muscle cells to the basement membrane. J. Neurochem. *96*, 53–64. https://doi.org/10.1111/j.1471-4159.2005.03539.x.

Morishima-Kawashima, M. (2001). Molecular analysis of tau deposited in the FTDP-17 brain. Rinsho Shinkeigaku *41*, 1107–1110, Japanese.

Nair, R.R., Solway, J., and Boyd, D.D. (2006). Expression cloning identifies transgelin (SM22) as a novel repressor of 92-kDa type IV collagenase (MMP-9) expression. J. Biol. Chem. *281*, 26424–26436. https://doi.org/10.1074/jbc.M602703200.

Navarro, V., Sanchez-Mejias, E., Jimenez, S., Muñoz-Castro, C., Sanchez-Varo, R., Davila, J.C., Vizuete, M., Gutierrez, A., and Vitorica, J. (2018). Microglia in Alzheimer's disease: activated, dysfunctional or degenerative. Front. Aging Neurosci. *10*, 140. https://doi.org/10.3389/fnagi.2018.00140. eCollection 2018.

Neddens, J., Temmel, M., Flunkert, S., Kerschbaumer, B., Hoeller, C., Loeffler, T., Niederkofler, V., Daum, G., Attems, J., and Hutter-Paier, B. (2018). Phosphorylation of different tau sites during progression of Alzheimer's disease. Acta Neuropathol. Commun. *6*, 52. https://doi.org/10.1186/s40478-018-0557-6.

Nelson, A.R., Sagare, A.P., and Zlokovic, B.V. (2017). Role of cluster in the brain vascular clearance of amyloid-β. Proc. Natl. Acad. Sci. U S A. *114*, 8681–8682.

Nirzhor, S.S.R., Khan, R.I., and Neelotpol, S. (2018). The biology of glial cells and their complex roles in Alzheimer's disease: new opportunities in therapy. Biomolecules *8*, 93. https://doi.org/10.3390/biom8030093.

Oddo, S., Caccamo, A., Shepherd, J.D., Murphy, M.P., Golde, T.E., Kayed, R., Metherate, R., Mattson, M.P., Akbari, Y., and LaFerla, F.M. (2003). Triple-transgenic model of Alzheimer's disease with plaques and tangles: intracellular Abeta and synaptic dysfunction. Neuron *39*, 409–421. https://doi.org/10.1016/s0896-6273(03)00434-3.

Owens, G.K., Kumar, M.S., and Wamhoff, B.R. (2004). Molecular regulation of vascular smooth muscle cell differentiation in development and disease. Physiol. Rev. *84*, 767–801. https://doi.org/10.1152/physrev.00041.2003.

Owens, G.K. (1995). Regulation of differentiation of vascular smooth muscle cells. Physiol. Rev. *75*, 487–517. https://doi.org/10.1152/physrev.1995.75.3.487.

Pettersen, E.F., Goddard, T.D., Huang, C.C., Couch, G.S., Greenblatt, D.M., Meng, E.C., and Ferrin, T.E. (2004). UCSF Chimera—a visualization system for exploratory research and analysis. J. Comput. Chem. *25*, 1605–1612. https://doi.org/10.1002/jcc.20084.

Popov, K.I., Makepeace, K.A., Petrotchenko, E.V., Dokholyan, N.V., and Borchers, C.H. (2019). Insight into the structure of the "unstructured" tau protein. Structure *27*, 1710–1715.e4. https://doi.org/10.1016/j.str.2019.09.003.

Pósfai, B., Cserép, C., Orsolits, B., and Dénes, Á. (2019). New Insights into microglia-neuron interactions: a neuron's perspective. Neuroscience *405*, 103–117. https://doi.org/10.1016/j.neuroscience.2018.04.046.

Rahimi, R., Nikfar, S., Sadeghi, M., Abdollahi, M., Moghaddam, R.H., and Farzaei, M.H. (2021). Effect of antihypertensive drugs on cognition and behavioral symptoms of patients with Alzheimer's disease: a meta-analysis. Curr. Pharm. Biotechnol. *22*, 1511–1519. https://doi.org/10.2174/1386207323666201211101720.

Rastelli, G., Rio, A.D., Degliesposti, G., and Sgobba, M. (2010). Fast and accurate predictions of binding free energies using MM-PBSA and MM-GBSA. J. Comput. Chem. *31*, 797–810. https://doi.org/10.1002/jcc.21372.

Rizzi, L., Rosset, I., and Roriz-Cruz, M. (2014). Global epidemiology of dementia: Alzheimer's and vascular types. Biomed. Res. Int. *2014*, 908915. https://doi.org/10.1155/2014/908915.

Rong, J.X., Shapiro, M., Trogan, E., and Fisher, E.A. (2003). Transdifferentiation of mouse aortic smooth muscle cells to a macrophage-like state after cholesterol loading. Proc. Natl. Acad. Sci. U S A. *100*, 13531–13536.

Roy, A., Kucukural, A., and Zhang, Y. (2010). I-TASSER: a unified platform for automated protein structure and function prediction. Nat. Protoc. *5*, 725–738. https://doi.org/10.1038/nprot.2010.5.

Royea, J., Lacalle-Aurioles, M., Trigiani, L.J., Fermigier, A., and Hamel, E. (2020). AT2R's (Angiotensin II Type 2 Receptor's) role in cognitive and cerebrovascular deficits in a mouse model of Alzheimer disease. Hypertension *75*, 1464–1474. https://doi.org/10.1161/HYPERTENSIONAHA.119.14431.

Salabei, J.K., Cummins, T.D., Singh, M., Jones, S.P., Bhatnagar, A., and Hill, B.G. (2013). PDGF-mediated autophagy regulates vascular smooth muscle cell phenotype and resistance to oxidative stress. Biochem. J. *451*, 375–388. https://doi.org/10.1042/BJ20121344.

San Martín, A., Lee, M.Y., Williams, H.C., Mizuno, K., Lassègue, B., and Griendling, K.K. (2008). Dual regulation of cofilin activity by LIM kinase and Slingshot-1L phosphatase controls platelet-derived growth factor-induced migration of human aortic smooth muscle cells. Circ. Res. *102*, 432–438. https://doi.org/10.1161/CIRCRESAHA.107.158923.

Steinbach, S.K., and Husain, M. (2016). Vascular smooth muscle cell differentiation from human stem/progenitor cells. Methods *101*, 85–92. https://doi.org/10.1016/j.ymeth.2015.12.004.

Streit, W.J., Braak, H., Xue, Q.S., and Bechmann, I. (2009). Dystrophic (senescent) rather than activated microglial cells are associated with tau pathology and likely precede neurodegeneration in Alzheimer's disease. Acta Neuropathol. *118*, 475–485. https://doi.org/10.1007/s00401-009-0556-6.

Tallquist, M., and Kazlauskas, A. (2004). PDGF signaling in cells and mice. Cytokine Growth Factor Rev. *15*, 205–213. https://doi.org/10.1016/j.cytogfr.2004.03.003.

Toledo, J.B., Arnold, S.E., Raible, K., Brettschneider, J., Xie, S.X., Grossman, M., Monsell, S.E., Kukull, W.A., and Trojanowski, J.Q. (2013). Contribution of cerebrovascular disease in autopsy confirmed neurodegenerative disease cases in the National Alzheimer's coordinating centre. Brain J. Neurol. *136*, 2697–2706. https://doi.org/10.1093/brain/awt188.

Tsuboi, Y. (2004). Clinical, genetic and pathological aspects of frontotemporal dementia and parkinsonism linked to chromosome 17 (FTDP-17). Rinsho Shinkeigaku *44*, 875–878, Japanese.

Turner, P.J. (2005). XMGRACE, Version 5.1. 19 (Center for Coastal and Land-Margin Research, Oregon Graduate Institute of Science and Technology).

Tyrrell, D.J., and Goldstein, D.R. (2021). Ageing and atherosclerosis: vascular intrinsic and extrinsic factors and potential role of IL-6. Nat. Rev. Cardiol. *18*, 58–68. https://doi.org/10.1038/s41569-020-0431-7.

Wallace, A.C., Laskowski, R.A., and Thornton, J.M. (1995). LIGPLOT: a program to generate schematic diagrams of protein-ligand interactions. Protein Eng. Des. Sel. *8*, 127–134. https://doi.org/10.1093/protein/8.2.127.

Wan, Y.W., Al-Ouran, R., Mangleburg, C.G., Perumal, T.M., Lee, T.V., Allison, K., Swarup, V., Funk, C.C., Gaiteri, C., Allen, M., et al. (2020). Meta-analysis of the Alzheimer's disease human brain transcriptome and functional dissection in mouse models. Cell Rep *32*, 107908. https://doi.org/10.1016/j.celrep.2020.107908.

Wang, G., Jacquet, L., Karamariti, E., and Xu, Q. (2015). Origin and differentiation of vascular smooth muscle cells. J. Physiol. *593*, 3013–3030. https://doi.org/10.1113/JP270033.

Wesseling, H., Mair, W., Kumar, M., Schlaffner, C.N., Tang, S., Beerepoot, P., Fatou, B., Guise, A.J., Cheng, L., Takeda, S., et al. (2020). Tau PTM profiles identify patient heterogeneity and stages of Alzheimer's disease. Cell *183*, 1699–1713.e13. https://doi.org/10.1016/j.cell.2020.10.029.

Wolfram Research, Inc. (2000). Mathematica, Version 12.1, Champaign, IL.

Xu, D., and Zhang, Y. (2011). Improving the physical realism and structural accuracy of protein models by a two-step atomic-level energy minimization. Biophys. J. *101*, 2525–2534. https://doi.org/10.1016/j.bpj.2011.10.024.

Yang, J., and Zhang, Y. (2015). I-TASSER server: new development for protein structure and function predictions. Nucleic Acids Res. *43*, W174–W181. https://doi.org/10.1093/nar/gkv342.

Zabel, M., Schrag, M., Crofton, A., Tung, S., Beaufond, P., Van Ornam, J., Dininni, A., Vinters, H.V., Coppola, G., and Kirsch, W.M. (2013). A shift in microglial β-amyloid binding in Alzheimer's disease is associated with cerebral amyloid angiopathy. Brain Pathol. *23*, 390–401. https://doi.org/10.1111/bpa.12005.

Zlokovic, B.V. (2011). Neurovascular pathways to neurodegeneration in Alzheimer's disease and other disorders. Nat. Rev. Neurosci. *12*, 723–738. https://doi.org/10.1038/nrn3114.

STAR★METHODS

KEY RESOURCES TABLE

REAGENT or RESOURCE	SOURCE	IDENTIFIER
Antibodies		
Anti-PDGF Receptor beta/PDGFR-β	Santa Cruz Biotechnology	sc-374573 Antibody (D-6)
Anti-PDGF-B	Santa Cruz Biotechnology	sc-365805 Antibody (F-3)
Anti-transgelin/ Alexa FluorÂ® 647	Santa Cruz Biotechnology	sc-53932 AF647 Antibody (6G6)
Anti-Tau	Santa Cruz Biotechnology	sc-32274 Antibody (Tau 46)
Anti-Tau (phospho S262)	Abcam	ab131354
APC anti-mouse CD68	BioLegend	137007 Antibody (FA-11)
Anti-human CD126 (IL-6Rα)	BioLegend	115803 Antibody (D7715A7)
Anti-human CD126 (IL-6Rα)	BioLegend	352801 Antibody (UV4)
Anti-MHC class II	Santa Cruz Biotechnology	sc-59322 Antibody (IBL-5/22)
Anti-NOS2	Santa Cruz Biotechnology	sc-7271 Antibody (C-11)
Anti-Tau [p Tyr18]	Novus Biologicals	NBP2-42402 Antibody (9G3)
Anti-Tau (phospho T205)	Abcam	ab4841
Anti-cofilin	Cell signaling	5175S Antibody (D3F9)
Anti-vinculin	Santa Cruz Biotechnology	sc-73614 Antibody (7F9)
Anti-CD45 Antibody	Santa Cruz Biotechnology	sc-1178 Antibody (35-Z6)
Anti-Iba1	Abcam	ab178846 Antibody (EPR16588)
Anti-MMP-9	Santa Cruz Biotechnology	sc-393859 Antibody (E-11)
Peptides		
Recombinant Tau P301L	rPeptide	rPeptide-T1014-1
Recombinant PGDFBB	Sigma	Sigma-GF149
Lipopolysaccharides	Sigma	Sigma-L9143
Experimental models: cell lines		
Human carotid Vascular Smooth Muscle Cells	Cell Applications	#3514K-05a
Human microglia	ScienCell	#1900
Experimental models: organisms/strains		
Tagln-cre mice	Jackson Laboratories	B6.Cg-Tg(Tagln-cre)1Her/J, Stock No: 017491
TdTomato mice	Jackson Laboratories	(B6.129S4-Gt(ROSA)26Sortm1Sor/J, Stock No: 003474
3xTgAD mice	Jackson Laboratories	B6;129-Tg (APPSwedish, tauP301L)1Lfa Psen1tm1Mpm/Mmjax, MMRRC Stock No: 34830-JAX
5XFAD mice	Jackson Laboratories	B6.Cg-Tg(APPSwFlLon,PSEN1*M146L*L286V) 6799Vas/Mmjax MMRRC Stock No: 008730
RNA-seq data		
ROSMAP	https://doi.org/10.7303/syn3388564	accession number: syn3388564
MSSM cohorts	https://github.com/th1vairam/ampadDiffExp/blob/df3efa793f379730bae6d4c9e62910fb2c37e525/gene_level_analysis/metaAnalysisForDiffExp.Rmd	PMID: 32668255

(*Continued on next page*)

Continued

REAGENT or RESOURCE	SOURCE	IDENTIFIER
Software and algorithms		
GROMACS	GROMACS development teams at Uppsala University	2020.4
VMD	University of Illinois at Urbana-Champaign	1.9.4a38
UCSF Chimera	University of California	1.14 build 42094
I-TASSER	Zhang Lab University of Michigan	5.1
ModRefiner	Zhang Lab University of Michigan	2011
XmGrace	Grace Development Team	Grace-5.1.25
LigPlot+	Thornton Group	v.1.4.5
APBS-PDB2PQR software suite	PoissonBoltzmann.org	v3.1.0
Wolfram Mathematica	Wolfram Research, Inc.	12.1
g_mmpbsa	Rashmi Kumari	2014

RESOURCE AVAILABILITY

Lead contact

Information and requests for resources may be directed to and will be fulfilled by the lead contact Christian L. Lino Cardenas (Clinocardenas@mgh.harvard.edu)

Material availability

This study did not generate new unique reagents.

Data and code availability

Any additional information required to reanalyze the data reported in this paper is available from the lead contact upon request.

METHODS DETAILS

Human Alzheimer disease, vascular SMC gene expression analysis

Bulk RNA-seq based gene expression data were analyzed from the dorsolateral prefrontal cortex (postmortem) from n = 414 individuals (n = 151 cognitively normal, non-demented controls and n = 263 AD subjects) in the Religious Orders Study and Rush Memory and Aging Project (ROSMAP) (PMID: 31340147). These data were downloaded from the AMP-AD Knowledge portal on the Synapse platform (Sage Bionetworks) using accession number: syn3388564 (https://doi.org/10.7303/syn3388564). A second validation data set containing RNA-seq data across 7 different brain regions from ROSMAP, Mayo and MSSM cohorts was analyzed (PMID: 32668255, https://github.com/th1vairam/ampad-DiffExp/blob/df3efa793f379730bae6d4c9e62910fb2c37e525/gene_level_analysis/metaAnalysisForDiffExp.Rmd). Briefly, differentially expressed genes (DEG) were detected in non-demented controls and AD brains using the *limma* package, after normalizing the expression values and removing batch effects and adjusting for covariates: age at death, sex, postmortem interval and APOE risk allele status. Genes were ranked by log2 fold change and posterior error probability. DEGs were then intersected with differentiated and modulated vascular SMC marker genes previously identified from single-cell RNA-seq of human coronary artery tissues (n = 34 subjects) (PMID: 31359001). These DEGs were also queried in single-nuclei RNA-seq of post-mortem human control and AD brain tissues (n = 24 subjects), courtesy of Dr. Philip De Jager and Dr. Vilas Menon (unpublished data). Github for detailed script (https://github.com/th1vairam/ampad-DiffExp/blob/df3efa793f379730bae6d4c9e62910fb2c37e525/gene_level_analysis/metaAnalysisForDiffExp.Rmd).

Mouse lines

All mice were cared under strict compliance with the Partners Institutional Animal Care and Use Committee (IACUC), regulated by the United States Department of Agriculture and the United States Public Health

Service and Institutional Animal Care and Use Committee of Massachusetts General Hospital, MA, USA. The Tagln-cre mice (B6.Cg-Tg(Tagln-cre)1Her/J, # 017491) were crossed with TdTomato mice (B6.129S4-Gt(ROSA)26Sortm1Sor/J, Stock No: 003474 |R26R) to generate VSMC-TdTomato positive cells. These mice were purchased from Jackson laboratories. Fixed brains of 3xTg-AD mice (B6;129-Tg (APPSwedish, tauP301L)1Lfa Psen1tm1Mpm/Mmjax, MMRRC Stock No: 34830-JAX) and B6.Cg-Tg(APPSwFlLon, PSEN1*M146L*L286V)6799Vas/Mmjax (5XFAD, Stock# 008730) were acquired from Jackson laboratories. For histology and immunofluorescence analysis, fixed brains were cryopreserved with sucrose and embed in OCT and sectioned (8μm). Both male and female mice were included in all analysis (ratio 1:1) In general, none significant changes or influence were observed between male and female under the same genetic background.

Cell lines for *in vitro* experiments

Primary human vascular smooth muscle cells from carotid of healthy donors were purchased from Cell Applications Inc. (#3514k-05a, neural crest origin). Human microglia were purchased from ScienCell Inc. (#1900, cortical origin). VSMC identity was validated by immunofluorescence staining of contractile markers, including SM22α and CNN1. To preserve cell identity, all experiments were carried out at passage number 1–5.

Ex-vivo experiments and AD-like models

For ex-vivo experiments, healthy brains from mice were collected and immediately, incubated in normal media (Cell Applications, #311-500) for 2 hrs in incubators maintained at 37°C and 5% CO_2. Then, brains were treated with neurotoxins to mimic AD-like conditions including with PDGF-BB (n = 4, 20ng/mL, Sigma-GF149), recombinant Tau P301L (n = 4, 20μg/mL, rPeptide-T1014-1) or LPS (n = 4, 0.8μg/mL, Sigma-L9143) for 48 hrs. For *in vitro* experiments, Human VSMCs and microglia cells were treated with PDGF-BB (n = 4, 15ng/mL, Sigma-GF149), recombinant Tau P301L (n = 4, 10μg/mL, rPeptide-T1014-1) or LPS (n = 4, 0.5μg/mL, Sigma-L9143) for 72 hrs, separately. Control groups (n = 4) were treated with DMSO at 0.01%. Cells were replenished with new growing media containing all three compounds every 24hrs.

Proteomic analysis

Whole brains were homogenized and approximately 400μg of total proteins were extracted using RIPA buffer (Thermo Fisher, CA, USA) and supplemented with 1X of protease inhibitor cocktail (Roche) according to the manufacturer's instruction, on ice for 30min. The protein concentration was determined by a BCA protein assay kit (Pierce Biothech), and then denatured protein samples were separated by SDS-PAGE followed by Coomassie staining. Then gel bands containing separated proteins were analyzed using an Orbitrap mass spectrometer (Thermo Scientific, CA, USA), as reported previously (Ibrahim et al., 2016). Ingenuity Pathway Analysis (IPA, Ingenuity Systems) software was used to identify potential canonical pathways associated with proteomics changes in the brains under AD-like conditions. The predicted activation state and activation Z-score are based on the direction of fold change values for those proteins in the input data set for which an experimentally observed causal relationship has been established (Krämer et al., 2014).

Quantitative flow cytometry

For the ex-vivo experiments, brains were homogenized and stained with anti-mouse CD68 (clone FA-110) and anti-mouse IL-6R (clone D7715A7) BioLegend. APC-conjugated anti-Feeder Cells (clone mEF-SK4) was purchased from Miltenyi Biotec. Cells were surface stained by incubation with the relevant antibodies diluted in PBS + 2% FBS for 20 minutes at room temperature, followed by 2 washes with PBS 2% FBS. When intracellular staining of signature cytokines was performed, cell suspensions were initially incubated for 3–5 hours at 37°C with RPMI T cell media containing 0.1% ionomycin (MilliporeSigma, I0634), 0.1% brefeldin A (BioLegend, 420601), 0.1% monensin (BioLegend, 420701), and 50 ng/ml of PMA (MilliporeSigma, P8139). After the incubation, surface staining was performed as indicated above, followed by cell fixation for 20 minutes at room temperature in light-protected storage with Fixation buffer (BD Biosciences, 554655). Upon fixation and being washed with PBS 2% FBS, cell suspension was permeabilized with 1× wash/permeabilization buffer (BD Biosciences, 554723; diluted in distilled water) and intracellular stained for 20 minutes at room temperature in light-protected storage. Absolute cell numbers were quantified using Precision Count Beads (BioLegend). Flow cytometry data was acquired on a LSRII (39) and analyzed using FlowJo software.

RNA extraction and qPCR analysis

Total RNA was extracted using a miRNeasy kit (Qiagen, Cat. No. / ID: 217084) following the manufacturer's protocol instructions. Briefly, 100 ng of total RNA was used as the starting template for cDNA synthesis. The cDNA was prepared by reverse transcription (RT), and gene expression was analyzed by quantitative PCR (qPCR) on a SYBR green system (Applied Biosystems). Expression results were analyzed by the ΔΔCT method, and GAPDH (encoding glyceraldehyde-3-phosphate dehydrogenase) was used as a housekeeping gene. Fold changes were calculated as the average relative to the control carotid as the baseline.

Wound healing assay

Human VSMC and microglial cell were seeded into silicone insert plates with a defined cell-free gap (Ibidi-labware, catalog no: CBA-120-5). VSMCs were stained with CellTracker™ Green CMFDA, (CMFDA, 5-chloromethylfluorescein diacetate, catalog number: C7025, Thermo Scientific). Microglia cells were stained with CellTracker™ Deep Red Dye (Catalog number: C34565, Thermo Scientific) and DAPI (4′,6-diamidino-2-phenylindole, Catalog number: D1306, Thermo Scientific). The VSMCs were treated with PDGF-BB (15ng/mL, Sigma-GF149), recombinant Tau P301L (10μg/mL, rPeptide-T1014-1) or LPS (0.5μg/mL, Sigma-L9143) for 72 hrs, followed by removal of insert. The migration of VSMCs and Microglia were observed for 0, 12, 24, 48hr and quantified as the % wound healing area occupied by cells. Images were taken on 20X magnification. No antiproliferative agents were added to the media, therefore wound healing in our assay reflects the combined activity of migration and proliferation.

Cell invasion assay and immunostaining

Briefly, 0.2 million VSMCs were seeded at the bottom of a trans-well plates and treated with PDGF-BB (15ng/mL, Sigma-GF149), recombinant Tau P301L (10μg/mL, rPeptide-T1014-1) or LPS (0.5μg/mL, Sigma-L9143) for 72 hrs, separately. And 0.3 million microglial cells were seeded at the top of the trans-well plate and labeled with a cell-permeable red dye (Catalog number: C34565, Thermo Scientific). Next both cell lines were incubated under normal conditions for 16 hrs followed by fixation of cells at the bottom of the plate with 4% of formaldehyde for 10 min. The migration of microglia cells was quantified as the number of red cells migrated towards VSMCs. In the reverse experiment of trans-well invasion assay, 0.3 million microglia were seeded at the bottom of trans-well and 0.2 million VSMCs were stained with a cell-permeable red dye (Catalog number: C34565, Thermo Scientific). Then microglia were treated with PDGFBB (15ng/mL, Sigma-GF149), recombinant Tau P301L (10μg/mL, rPeptide-T1014-1) or LPS (0.5μg/mL, Sigma-L9143) for 72 hrs as mentioned above. For 3D microscopy immunofluorescence analysis primary antibodies against CD68 (Santa cruz biotechnology, sc-20060) MHC-II (Santa Cruz biotechnology, sc-59322) and iNOS (Abcam, ab15323) were used at 1:100 concentrations. For the 2D immunofluorescence analysis primary antibodies against PDGFRB (Santa Cruz biotechnology, sc-374573) and MMP9 (Santa Cruz biotechnology, sc-393859 AF488) were used at 1:50 concentrations. In the indirect stimulation assay in Figure 3D, VSMCs were labeled with a permeable red dye (Catalog number: C34565, Thermo Scientific) overnight followed by treatment with PDGF-BB (15ng/mL, Sigma-GF149), recombinant Tau P301L (10μg/mL, rPeptide-T1014-1) or LPS (0.5μg/mL, Sigma-L9143) for 72 hrs. Then VSMCs were tyrosinated and co-cultured with microglia under normal condition for 24hrs before fixation with 4% of formaldehyde for 10 min. Then cells were permeabilized with 0.5% of triton-x for 10 min and blocked with donkey serum at 10% for 1h followed by primary antibody incubation at 4°C overnight. Secondary antibodies were used at 1:400 and slides were mounted with diamond mounting medium containing DAPI (Thermo Fisher). Cells were visualized with the Leica TCS SP8 confocal microscopy station and pictures were digitized with the Leica Application Suite X software. Two-dimensional and white-light images were analyzed using ImageJ software.

Immunoblotting

Total protein lysates were prepared using NE-PER Kit (Pierce, Rockford, IL, USA) and supplemented with 1X of protease inhibitor cocktail (Roche) according to the manufacturer's instruction. For detection of proteins 25 μg of total extracts were mixed with denaturing buffer (1× Laemmli loading buffer with 10% of β-mercaptoethanol) and analyzed by SDS–PAGE/Western blot. Separated proteins were transferred onto a 0.45-μm pore size nitrocellulose membrane (Millipore) using the iBlot transfer system (Novex, Thermo Fisher, USA). Membranes were incubated with primary antibodies diluted from 1:500 to 1:1000, followed by TBS-T washes and incubation with HRP (horseradish peroxidase)—conjugated secondary antibodies (GE Healthcare). The signal was visualized by enhanced chemiluminescence with Luminata Forte Western

HRP Substrate (Millipore) and the ImageQuant LAS 4000 imaging system. The following antibodies were used: anti-p-TauS262 (Abcam, ab131354), anti-total Tau (Abcam, ab76128), anti-p-Tau-T205 (Santa Cruz biotechnology, sc-73614), anti-VCL (Abcam, ab254410) and anti-p-Tau Y18 (GeneTex, GTX54658), Anti-CFL-1 (Abcam, ab42824). Immunoblot uncut membranes are provided in DATA S1.

Computational details

System building, structural refinements and molecular dynamic simulations (MDS). The 2N4R Tau sequence (441 aa), was used to build the wild-type Tau protein 3D structure using the I-TASSER server (Roy et al., 2010; Yang and Zhang, 2015; Yang and Zhang, 2015). The TauP301S and TauP301L were built based on wild-type 3D model by performing 301 site direct mutagenesis using UCSF Chimera software (Pettersen et al., 2004). Then the structural refinement was carried out to avoid residues overlapping using ModRefiner server (Xu and Zhang, 2011). Classical MD simulations were performed using GROMACS 2020.4 package (Abraham et al., 2015) with the OPLS-AA force field parameters (Jorgensen et al., 1996). All three Tau protein systems were built in a triclinic simulation box considering periodic boundary conditions (PBC) in all directions (x, y, and z) (Table S3). Then, they were solvated using the TIP4P water model (Jorgensen and Madura, 1985), and Cl-ions were used for neutralization of total charge in the simulation box. Mimicking of physiological conditions was performed by ionic strengthening with the addition of 150mM NaCl. The distance of the protein surfaces to the edge of the periodic box was set at 1.5nm. And 1 fs step was applied to calculate the motion equations using the Leap-Frog integrator (Hockney et al., 1974). The temperature for proteins and water-ions in all simulations was set at 309.65 K using the modified Berendsen thermostat (V-rescale algorithm) (Berendsen et al., 1984) with a coupling constant of 0.1 ps. Pressure was maintained at 1bar using the Parrinello-Rahman barostat (Bussi et al., 2007) with a compressibility of 4.5x10−5 bar-1 and a coupling constant of 2.0 ps. Particle mesh Ewald method (Ewald, 1921) was applied to long-range electrostatic interactions with a cutoff equal to 1.1nm for non-bonded interactions with a tolerance of 1x105 for contribution in real space of the Tau 3D structures. The Verlet neighbor searching cutoff scheme was applied with a neighbor-list update frequency of 10 steps (20 fs). Bonds involving hydrogen atoms were constrained using the Linear constraint solver (LINCS) algorithm (Hess, 2008). Energy minimization in all simulations was performed with the steepest descent algorithm for a maximum of 100,000 steps. For the equilibration process, we performed two steps, one step of dynamics (1ns) in the NVT (isothermal-isochoric) ensemble followed by 2 ns of dynamics in the NPT (isothermal-isobaric) ensemble. Then the final simulation was performed in the NPT ensemble for 500 ns followed by the analysis of the Tau 3D structures and their energy properties.

Structural and energetic analysis of tTau 3D protein structures. All MD trajectories were corrected, and the Tau 3D structures were recentering in the simulation boxes. RMSD, RMSF, radius of gyrations, H bonds, residue distances, and solvent accessible surface area analyses were performed using the Gromacs tools and results were plotted using XMGrace software (Turner, 2005). For visualization of Tau 3D structures, we used the UCSF Chimera, VMD software packages (Humphrey et al., 1996). Analysis of atomic interactions and 2D plots was generated using the LigPlot software packages (Wallace et al., 1995). The electrostatic potential (ESP) surfaces were calculated using the APBS (Adaptive Poisson-Boltzmann Solver) software, and the PDB2PQR software was used to assign the charges and radii to protein atoms (Baker et al., 2001; Dolinsky et al., 2004). FEL maps were generated to visualize the energy associated with the conformational structure of all three Tau proteins during the molecular dynamic simulation. FEL maps were generated using the RMSD and radius of gyration as atomic position variables respect to its average structure. FEL maps were plotted using using gmx sham and figures were built using Wolfram Mathematica 12.1 (Wolfram Research, Inc., 2020).

Calculation of binding free energy. The Molecular Mechanics Poisson-Boltzmann Surface Area (MM/PBSA) calculation of free energies and energy contribution by individual residues were carried out to analyze the impact of amino acid substitutions (P301S and P301L) in the R2-R3 domains using the last 50ns of MD trajectories and the g_mmpbsa package (Kumari et al., 2014). Therefore, the interacting energy was calculated using the following equation:

$$\Delta G_{int} = G_{Tau} - (G_1 + G_2)$$

where the terms G_1 and G_2 are the free energy of the different sites of the Tau protein, and G_{Tau} is the free energy of entire Tau 3D structure. In this context, the free energy of each term was calculated as follow:

$$G_x = E_{MM} + G_{solv} - TS$$

where E_{MM} is the standard mechanical energy (MM) produced from bonded interactions, electrostatic interactions, and van der Waals interactions. G_{solv}, is the solvation energy that includes the free energy contributions of the polar and nonpolar terms. In this work, we used the solvent accessible volume (SAV) model to calculate the nonpolar term. The TS term refers the entropic contribution and was not included in this calculation due to the computational costs (Brown and Muchmore, 2009; Rastelli et al., 2010; Kumari et al., 2014). Finally, 309 Kelvin (K) of temperature was used as the default parameter in all our calculations.

QUANTIFICATION AND STATISTICAL ANALYSIS

Results are given as Mean ± SD. Student's test was applied to determine the statistical significance of difference between control and treated groups (*$p < 0.05$, **$p < 0.01$ and ***$p < 0.001$). For all experiments at least three replicates were performed. Two-way analysis of variance (ANOVA) was used to analyze healing versus time of Figure 2D (95% confidence interval is plotted). p values represent one-way ANOVA followed by Tukey's honestly significant difference (HSD) post-hoc test. All graphs were produced using GraphPad Prism 8.0.